Copyright Warning & Restrictions

The copyright law of the United States (Title 17, United States Code) governs the making of photocopies or other reproductions of copyrighted material.

Under certain conditions specified in the law, libraries and archives are authorized to furnish a photocopy or other reproduction. One of these specified conditions is that the photocopy or reproduction is not to be "used for any purpose other than private study, scholarship, or research." If a, user makes a request for, or later uses, a photocopy or reproduction for purposes in excess of "fair use" that user may be liable for copyright infringement,

This institution reserves the right to refuse to accept a copying order if, in its judgment, fulfillment of the order would involve violation of copyright law.

Please Note: The author retains the copyright while the New Jersey Institute of Technology reserves the right to distribute this thesis or dissertation

Printing note: If you do not wish to print this page, then select "Pages from: first page # to: last page #" on the print dialog screen

ABSTRACT

NANOCARBON IMMOBILIZED MEMBRANE FOR SEPARATION AND ANALYSIS

by
Madhuleena Bhadra

Membrane processes classically cover a wide range of applications associated with various aspects of separation and purification. Over the last few years, membrane based processes have received much interest due to their compact and modular architecture, low energy consumption and cost effective separation. With the development of diverse nanomaterials which can serve as nanosorbents, or provide specific morphology for selective solute transport, recent years have witnessed the emergence of nanocarbon based membranes that can address some of the limitations of conventional membrane processes and make feasible the next generation of breakthroughs.

The objective of this research is the exploration of carbon nanotube immobilized membrane (CNIM) for performance enhancement in two lead membrane separation processes, namely, membrane extraction and membrane distillation. A state of the art of the implementation of carbon nanotube membranes on polar membranes for extraction of emerging polar analytes is addressed. Succeeding investigation and experimental studies performed on hydrophobic and hydrophilic functionalized carbon nanotube membranes for sweep gas membrane distillation and direct contact membrane distillation is also studied. With respect to the conventional membrane distillation membrane, the CNIM membrane demonstrates several interesting properties, which aid in improving the overall desalination performance. Besides noteworthy enhancement in flux in CNIM, further

investigations are carried out utilizing emerging nanocarbons, namely, detonation nanodiamonds (DND).

Overall, it is demonstrated that the nanocarbon immobilized membranes show enhanced performance with significantly higher levels of flux enhancement and enrichment, thereby improving the overall membrane selectivity.

NANOCARBON IMMOBILIZED MEMBRANE FOR SEPARATION AND ANALYSIS

By

Madhuleena Bhadra

A Dissertation
Submitted to the Faculty of
New Jersey Institute of Technology
in Partial Fulfillment of the Requirements for the Degree of
Doctor of Philosophy in Chemistry

Department of Chemistry and Environmental Science

May 2014

APPROVAL PAGE

NANOCARBON IMMOBILIZED MEMBRANE FOR SEPARATION AND ANALYSIS

Madhuleena Bhadra

Dr. Somenath Mitra, Dissertation Advisor — Date
Distinguished Professor of Chemistry and Environmental Science, NJIT

Dr. Carol Venanzi, Committee Member — Date
Professor Emeritus of Chemistry and Environmental Science, NJIT

Dr. Edgardo T. Farinas, Committee Member — Date
Associate Professor of Chemistry and Environmental Science, NJIT

Dr. Haidong Huang, Committee Member — Date
Assistant Professor of Chemistry and Environmental Science, NJIT

Dr. Pradyot Patnaik, Committee Member — Date
Consultant, Radiance, New Jersey

BIOGRAPHICAL SKETCH

Author: Madhuleena D Bhadra

Degree: Doctor of Philosophy

Date: May 2014

Undergraduate and Graduate Education:

- Doctor of Philosophy in Chemistry
  New Jersey Institute of Technology, Newark, NJ, 2014
- Master of Science in Chemistry
  New Jersey Institute of Technology, Newark, NJ, 2009
- Bachelor of Science in Chemistry
  St. Xaviers College, Mumbai, India, 2006

Major: Chemistry

Peer Reviewed Publications:

Madhuleena Bhadra, Ornthida Sae Khow and Somenath Mitra, "Effect of carbon nanotube functionalization in micro-solid-phase extraction (μ-SPE) integrated into the needle of a syringe", Analytical. Bioanalytical. Chemistry. 2011, 402, 1029-1039.

Madhuleena Bhadra and Somenath Mitra,"Carbon nanotube immobilized polar membranes for enhanced extraction of polar analytes", Analyst. 2012, 137, 4464-4468.

Madhuleena Bhadra and Somenath Mitra, "Nanostructured membranes in analytical chemistry", Trends in Analytical Chemistry. 2013, 45, 248- 263.

Madhuleena Bhadra, Sagar Roy and Somenath Mitra, "Enhanced desalination using carboxylated carbon nanotube membrane", Separation and Purification Technology. 2013, 120, 373-377.

Madhuleena Bhadra, Sagar Roy and Somenath Mitra, "Nanodiamond immobilized membranes for enhanced desalination via membrane distillation", Desalination. 2014, 341, 115–119.

Sagar Roy, Madhuleena Bhadra and Somenath Mitra, "Enhanced desalination via functionalized carbon nanotube immobilized membrane in direct contact membrane distillation", Separation and Purification Technology. In review.

Madhuleena Bhadra, Sagar Roy and Somenath Mitra, "Flux enhancement in direct contact membrane distillation by implementing carbon nanotube immobilized membrane", ACS Applied Materials and Interfaces. In review.

Madhuleena Bhadra and Somenath Mitra, "Bilayer functionalized carbon nanotube immobilized membrane for direct contact membrane distillation", In preparation.

Ken Gethard, Ornthida Sae khow and Madhuleena Bhadra, "Concentration of trace inorganics in aqueous streams using carbon nanotube enhanced membrane distillation", In Preparation.

Madhuleena Bhadra and Somenath Mitra, "Desalination across graphene oxide immobilized membrane for direct contact membrane distillation", In preparation.

Book Chapter:

Madhuleena Bhadra and Somenath Mitra, "Advanced nanostructured membranes for desalination", Nanotechnology Applications for Clean Water : Solutions for improving water quality (2nd edition). Release June 2014.

Patent:

Madhuleena Bhadra, Sagar Roy and Somenath Mitra, 13-068 - Application # 61/886,771. Enhanced desalination using carboxylated carbon nanotube immobilized membranes.

To my mom, Sujata Bhadra and dad, Dilipkumar Bhadra - You are my inspiration

To my husband, Kyle - Couldn't have done it without you

ACKNOWLEDGMENT

I wish to express my sincere gratitude to my dissertation advisor, Dr. Somenath Mitra, for his guidance in my PhD journey that consists of challenges and interests. I appreciate what I have learned from him, not only in terms of the broad knowledge, sharp scientific instinct and creative ideas, but also the optimistic and confident personalities. I am very grateful to my committee members Dr. Carol Venanzi, Dr. Haidong Huang, Dr. Pradyot Patnaik and Dr. Edgardo Farinas for their insighful guidance and serving on my dissertation committee.

I greatly appreciate the help of Ms. Clarisa Gonzalez- Lenahan, as well as the staff of the Graduate Studies Office and faculty throughout my study at NJIT. I am grateful to Electric Power Research Institute (EPRI) for financial support. I also want to thank Celgard for their kind donation of membrane material. Thanks to Gayle Katz, Genti Price and Yogesh Gandhi of the Department of Chemistry and Environmental Science for their help.

Additionally, I would like to thank Dr. Ornthida Sae Khow and Dr. Ken Gethard for getting me started with my research. A very special thanks and appreciation to Dr. Sagar Roy for all his support, assistance and collaboration. Finally, I am grateful to my mom, dad, and my husband, for their continuous love and support during this adventure.

TABLE OF CONTENTS

TABLE OF CONTENTS
(Continued)

TABLE OF CONTENTS
(Continued)

LIST OF TABLES

LIST OF FIGURES

LIST OF FIGURES
(Continued)

LIST OF FIGURES
(Continued)

LIST OF FIGURES
(Continued)

Figure **Page**

CHAPTER 1

INTRODUCTION

1.1 Membrane Separation and Extraction

Membranes have been used in many industrial scale separations, such as, gas purification, water treatment, desalination, filtration, dialysis, dehumidification, osmosis, reverse osmosis, and electrodialysis [1]. They have also been used to achieve a variety of analytical scale separations that include extraction, concentration and cleanup. Being semi permeable, they primarily function as a barrier that allows the selective transport of a solute. In analytical applications, this allows the enrichment of the species of interest and their removal from the sample matrix. The movement of the analytes of interest may be driven by a chemical, pressure or an electrical potential gradient [2]. In current years, membrane techniques have vastly developed numerous analytical techniques by facilitating separations without the mixing of two phases, thus eliminating problems such as emulsion formation and high solvent usage. These techniques can allow simultaneous extraction and enrichment of analytes as well, and facilitate trace level analysis while consuming small amounts of solvents. Membrane extraction has been applied to a wide range of analytes including biological molecules, metals and organic pollutants [3-6]. They have also been prolifically used in diverse environmental media that include air and water, and at the same time are becoming popular in biomedical applications with matrices such as, urine, blood and blood plasma to analyze drugs and their metabolites [7-8]. Such media are complex and usually require tedious and multiple sample preparation steps. Furthermore, micro scale sample volumes, particularly in liquid membranes lead to high enrichment in order of thousands [9] and detection limits in the

range of sub ppb levels. As a result, techniques such as membrane-based micro extraction often referred to as hollow fiber-liquid phase micro extraction (HF-LPME) are seen as an alternative to solid-phase extraction (SPE), solid-phase micro extraction (SPME) or traditional liquid-liquid extraction (LLE). It is also worth mentioning that membrane extractors have also been micro fabricated.

Applications of membrane extraction are quite diverse and encompass different types of membranes, module designs as well as the variation in extraction chemistry [10]. Though it is conceivable that they can be collectively used to achieve any sample preparation, the key to their success lies in achieving high selectivity and flux; two parameters that often tend to be divergent. Consequently, there is tremendous interest in developing newer membranes to suit specific applications.

In an effort to develop the next generation membrane with high permeability and selectivity, much effort has gone into the design of both membrane materials and architecture [11]. Recent interest has been in the use of nanomaterials and nanostructures to form nanocarbon membranes, which have successfully engineered pore size, surface area as well as physical and chemical properties such as sorbent characteristics and interactions with solutes [12]. A variety of nanomaterials including carbon nanotubes (CNTs), zeolites, and gold have been incorporated in membrane structures to investigate the implementation of nanomaterials in membranes and their applications in various separation applications.

1.2 Separation Principles

A membrane is a selective barrier through which different gases, vapors and liquids permeate at varying rates. The membrane aids the contacting of two phases at the membrane interface. Molecules move through membranes by the process of diffusion and are driven by a concentration (ΔC), pressure (ΔP) or electrical potential (ΔE) gradient (Figure 1.1). The interesting aspect of this technique is that both the donor and acceptor can flow continuously leading to the development of automated, real-time monitoring techniques. This diffusion-based transport can be expressed by Fick's first law of diffusion:

$$J = -D\, dc/dx \qquad (1.1)$$

where J is the flux (g/cm^2s), D is the diffusion coefficient (cm^2s), and dc/dx is the concentration gradient. However there are membrane factors that affect the rate of diffusion such as thickness and concentration. Their effect can be described by:

$$J = D\,(c_{is} - c_{il})/L \qquad (1.2)$$

where c_{is} is the concentration of i at outer membrane surface, c_{il} is the concentration of i in the membrane lumen and L is the thickness of the membrane wall.

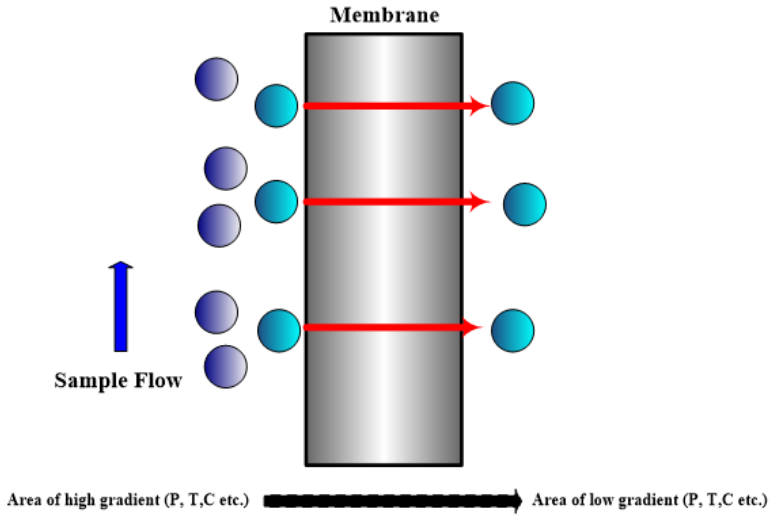

Figure 1.1 Schematic representation of permeation across a membrane. Pressure, temperature or concentrations are examples of gradients that provide driving force.

Permeation across non-porous dense membranes comprises of several steps: 1. partitioning of the analyte in the membrane; 2. diffusion under a concentration gradient, and finally, 3. partitioning into the extractant phase. There are also boundary layers present on the membrane surfaces that provide an additional barrier to mass transfer. These steps are illustrated in Figure 1.2.

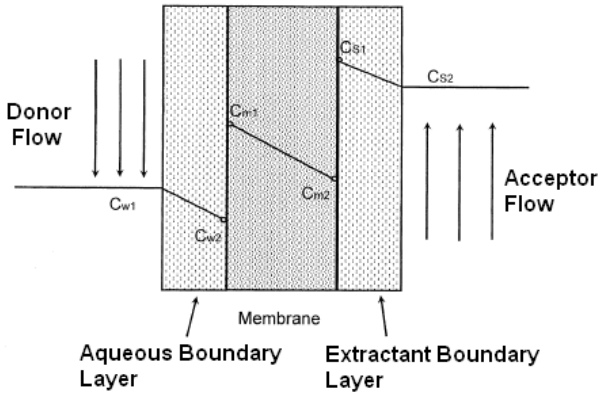

Figure 1.2 Concentration profile in an extraction process, where C_w, C_m and C_s refer to analyte concentration in water, membrane and the extractant phases respectively.

It is imperative to note here that K decreases with temperature, while D increases under the same conditions. Consequently, increasing temperature does not always increase flux, and an optimum temperature must be determined where the flux is greatest. It is essential to note that the diffusion coefficient is a function of concentration. Thus, theoretical predictions in analytical applications are a difficult task where concentration varies by orders of magnitude. The enrichment factor (EF) and extraction efficiency (EE) are the two major parameters used to evaluate the effectiveness of a particular extraction. The EF may be defined as the ratio of analyte concentration in the extract to that in the initial donor:

$$EF = \frac{C_a}{C_s} \tag{1.3}$$

where, $\mathbf{C_a}$ is the analyte concentration in the final extract and $\mathbf{C_s}$ is the analyte concentration in the original sample. The EE refers to the fraction of analyte that is extracted into the acceptor such that:

$$EE = \frac{m_a}{m_d} = \frac{C_a}{C_d} x \frac{V_a}{V_d} = EF \frac{V_a}{V_d} \tag{1.4}$$

where, n_s and n_w are the analyte mass in the final extract and in the original water sample, Vs and Vw are the volume of the concentrated extract and the original water sample respectively.

The two most commonly used membrane-based liquid phase extraction techniques in analytical applications are: 1) Supported Liquid Membrane Extraction (SLME) and 2) Liquid-liquid membrane extraction (LLME). In LLME, the analyte is extracted from an aqueous solution into an organic one and hence it is a two-phase organic-aqueous system. It is essentially liquid-liquid extraction where the two phases contact at the membrane pores. SLME is a versatile membrane extraction technique for highly polar, acidic, basic and ionic analytes that shows extremely high enrichment factors in thousands and detection limits in sub ppb levels. Since SLME is a three-phase extraction technique, where the analytes are extracted from an aqueous sample into another aqueous phase through an organic extractant [13], compared to LLME it offers higher selectivity, donor/acceptor ratio and extraction efficiency. There also are many other possibilities.

While LLME and SLME are good for semi volatile analytes, extracting into a gas phase is the best method for separating volatile organics. Pervaporation refers to the separation of a liquid mixture by partial vaporization through a porous or a non-porous membrane. The sample flows on one side of the membrane, and the volatile species permeate as vapors in a flow of sweep gas or vacuum. Overall, flux through a pervaporation membrane can be expressed in terms of the partial vapor pressure on either sides of the membrane such that:

$$J_a = P_a^G \frac{(Pa_o - Pa_l)}{L} \qquad (1.5)$$

where, J is flux, L is membrane thickness, P_a^G is gas separation permeability coefficient, Pa_o is partial vapor pressure of donor, Pa_l is partial vapor pressure in acceptor. The pervaporated organics have been concentrated using a sorbent trap to be followed by thermal desorption into a gas chromatographic system [14]. This approach has been used for the analysis of volatile organic compounds in air as well as aqueous samples. A more recent application has been the development of membrane distillation [15]. Here the water (or a solvent) is selectively permeated out of a hollow fiber membrane leading to a concentrated solution. This has been successfully used in the concentration of pharmaceutical compounds.

1.3 Automation of Membrane Separation

A major advantage of membrane processes is that the sample and the extractant can be contacted continuously, thus providing the basis for a continuous, real-time process leading to automation and online analysis. A fully automated analytical system can be built to perform a complete analysis where the membrane serves the purpose of selective extraction and sample introduction. In general, on-line methods reduce sample handling and hence the probability of analytical errors and sample loss. They have been directly interfaced with gas chromatography (GC), liquid chromatography (LC), mass spectrometry (MS), ion chromatography (IC), atomic absorption spectroscopy, inductively coupled plasma atomic emission spectroscopy (ICP-AES) and capillary electrophoresis (CE) [16-18].

Online membrane extraction can be directly interfaced with HPLC to provide high enrichment. After the extraction is completed, the contents of the acceptor channel is transferred directly into the injection loop and subsequently injected into the HPLC column. A major development in the above field with online automation has been the development of total analytical system (TAS) that refers to the integration of sample preparation and concentration into one system [19]. In principle, the membrane extraction served as the separation and the initial enrichment step, while the pervaporation served as the preconcentration step. Typically, the acceptor flowed inside the lumen of hollow fiber membrane extractor, while the water sample (donor) flowed counter-current on the shell side. Following this, the stripping gas selectively removed some of the solvent from the extract resulting in a more concentrated extract for HPLC analysis.

A membrane based, on-line concentration technique using pevaporation has been developed. With this technique selective solvent permeation leads to analyte preconcentration. The dilute solution flows into a shell and tube module, and an inert gas flows on the permeate side. The membrane preferentially allows migration of the solvent across the membrane and a more concentrated solution remains in the lumen. This was shown to be applicable to both polar and non-polar membranes for analytes such as, atrazine, pentachlorophenol, naphthalene and biphenyl. The instrumentation for analysis can be automated to concentrate either multiple samples or interfaced with chromatography.

1.4 Membrane Distillation

Membrane distillation (MD) is a thermally driven, membrane based separation process which is a hybrid between thermal desalination and micro porous hydrophobic membrane was introduced in late 1960s. In MD, hot aqueous solution is passed through the lumen of a porous hydrophobic hollow fiber [20]. While preventing the transport of the liquid phase, MD relies on the net flux of water vapor from the warm to the cool side of the membrane. Typically, MD is carried out at 60-90ºC, which is notably lower than conventional distillation. As a result, it has the prospective to generate high quality drinking water using only low temperature heat sources such as waste heat from industrial processes and solar energy. Customarily, MD has received much attention as an alternative to thermal distillation and reverse osmosis desalination of sea and brackish waters. Various types of MD have been known for the past several years: direct contact MD (DCMD), air gap MD (AGMD), sweeping gas MD (SGMD), and vacuum MD (VMD) [21]. These terms refer to the permeate side of the membrane. In all cases, the feed is in direct contact with the membrane. In DCMD, both sides of the membrane contact a liquid phase. The liquid on the permeate side is used as the condensing medium for the vapors. In AGMD the condensed permeate is not in direct contact with the membrane, in SGMD a sweep gas is used to remove the water vapor and in VMD the permeate side has vacuum.

A key component in MD is the membrane itself because it determines both flux and selectivity. As of now the throughput of MD processes are relatively low, since two major factors were impeding its development namely; membranes with adequate characteristics and unfavorable economics of the process compared to RO. Recent

developments convey the coupling of MD with waste heat and renewable energy driven systems such as geothermal and solar energy provide for greater efficiency. Some advantages of MD include the ability to operate at lower temperature, lower pressure, and the ability to handle higher brine concentrations. In conclusion, the structural design and chemistry of membranes engineered for MD are critical to achieve high performance.

Typically, in MD processes, the penetration of liquid into the membrane's pores must be avoided, as this causes the pore to lose its hydrophobic capacity. As long as the feed pressure is kept low enough, a critical threshold known as the breakthrough pressure is not reached. The LaPlace equation describes the relation between pore size and the breakthrough pressure:

$$\Delta P = -\frac{2\mathrm{O}y\cos\theta}{r} \tag{1.6}$$

where y is the interfacial tension, O is a geometric factor related to the pore structure, and Θ is the liquid solid contact angle. This angle increases with increasing polarity difference between the polymeric membrane and the liquid. For hydrophobic membranes, the contact angle is greater than 90º.

The water transport involves evaporation into the bulk solution with higher water activity, followed by vapor transport in the gas phase and then condensation in the solution with the lower water activity. The water flux is proportional to the water vapor pressure difference across the membrane controlled by the water vapor activity difference. As mass transfer proceeds a boundary layer is formed on each side of the membrane. The water activity difference between both membrane interfaces is lower

than the bulk feed resulting in the reduction of the driving force. The flux in the boundary layers can be related to the mass transfer coefficients k_1 and $k_{2\ by:}$

$$J_w = k_1(a_1 - a_{m1}) = k_2(a_{m2} - a_2) \tag{1.7}$$

where a_i is the bulk water activity and a_{mi} is the water activity at the membrane interface. MD is similar to pervaporation in that the driving force is determined by a vapor pressure difference on either side of the membrane, however in MD there is also a simultaneous heat transfer involved. Typically, MD is depicted as having a liquid-vapor interface forming at the entrance to the membrane's pores. Only a gaseous phase is present inside the pores and as long as a pressure gradient is maintained, the vapor will be transported. A depiction of the membrane distillation process is shown in Figure 1.3.

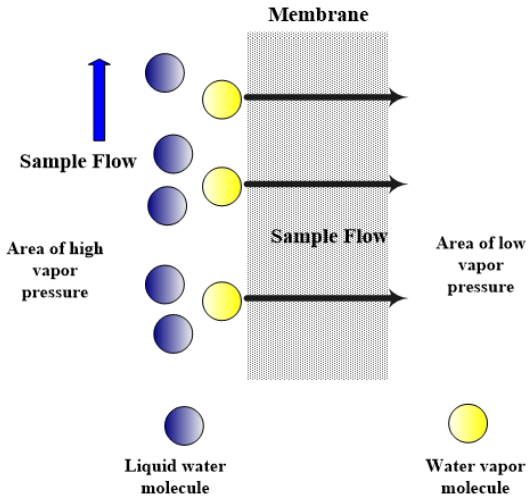

Figure 1.3 Representation of membrane distillation, vapor flows from an area of higher vapor pressure to an area of lower vapor pressure across a hydrophobic membrane.

Since MD is a thermally driven process, both heat and mass transport are involved simultaneously, and heat transfer is often the rate-limiting step. There are two essential mechanisms accountable for the heat transfer across the membrane. The first is conduction through the membrane material and the vapor within the membrane pore, and transfer of the heat of vaporization coupled with the vapor flux. On the whole, Heat transfer in MD can be considered in three steps. The first is convective heat transfer across the boundary layer to the membrane surface from the heated solution. The second is heat transfer across the membrane by conduction and assembling the vapor flow all the way through the pores. The third is the convective heat transfer from the membrane surface of the permeate side across the boundary layer to the bulk permeate solution. The heat transfer can be described by:

$$Q = J\Delta H_v + \frac{k_m}{\mathrm{M}}(T_{m1} - T_{m2}) \qquad (1.8)$$

where J is the flux, M is the membrane thickness, ΔH_v is the latent heat of evaporation, k_m is the thermal conductivity of the porous membrane and T_{m1} and T_{m2} at the hot and cold membrane surfaces.

In MD process, the evaporation efficiency is defined as the ratio between the heat which contributes to evaporation and the total heat exchanged by the feed. The total heat

exchanged by the feed is the difference between the sensible heat of the incoming feed stream ($Q_{1\text{-}in}$) and the sensible heat of the outgoing feed stream ($Q_{1\text{-}out}$). A large amount of heat is used to vaporize the solution, which further results in a temperature difference between the bulk solution and the membrane surface, causing a temperature polarization. This temperature polarization causes a significant loss in the driving force of the mass transfer through the membrane.

With MD, mass transfer is alienated into three steps, mass transfer in the feed boundary layer, mass transfer across the membrane and mass transfer in the permeate boundary layer. The Dusty gas model (DGM) is generally used to explain mass transfer across a membrane's pore in MD. With the DGM, the pore's medium is viewed as a grouping of uniformly distributed dust particles held stationary in space. The presence of gas-surface interactions considers the gas molecules as large particles. This model is composed of four components: molecular (Fickian) diffusion, Knudsen diffusion, surface diffusion and viscous flow as shown in Figure 1.4. Molecular diffusion is used in circumstances when collisions between molecules play the main role in mass transport. The Knudsen diffusion model is followed whenever collisions between molecules and the pore's wall are the dominant transport mechanism. Surface diffusion represents flow when a solute molecule adsorbs on the surface of the pore and then hops from one site to another based on interactions between the surface and the molecules. Viscous flow is the general flow of a gas across a channel under conditions where the mean free path is small in comparison to the transverse section of the channel and the flow characteristics are determined mainly by collisions between the gas molecules.

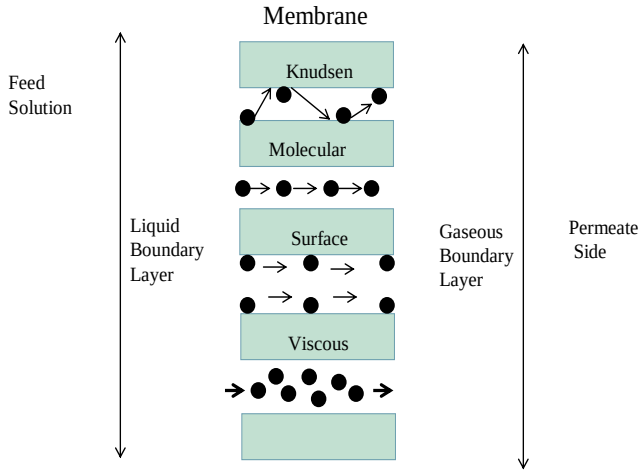

Figure 1.4 Membrane distillation diffusion mechanisms across hydrophobic membrane pores.

Ordinarily in MD, mass transport is typically explained in terms of only Knudsen or molecular diffusion. As membrane pore size decreases (to less than 0.2 micron), Knudsen forces outweigh, and conversely as pore diameter increases, molecular diffusion is the dominant transport mechanism. To date, surface diffusion and viscous flow have not been considered as foremost contributors in MD. Further, the mass transfer boundary layers at the bulk feed-membrane and permeate-membrane interfaces are thought to result in negligible contributions to overall mass transfer resistance.

Membranes those are most apposite for MD processes ought to have the following properties:

- Small thickness and low tortuosity
- Low thermal conductivity of the membrane material
- High porosity to lower conductive heat flux and increase water vapor transport
- Reasonable pore size, but balanced by preventing membrane pore wetting

- Low surface energy or high hydrophobicity so the membrane is applicable under high pressure.

1.5 Nanocarbon Membranes

As previously mentioned, the two important membrane characteristics are their flux and selectivity. These are controlled by chemical and physical characteristics, morphology as well as the presence of and absence of pores. It is well known that conventional polymeric and ceramic membranes have great potential in a wide range of industrial as well as analytical applications. The limitations in membrane applications come from selectivity and permeability. Typically they appear to be reciprocal of each other; higher selectivity tends to decrease flux. For example larger pore size may increase flux but reduce selectivity. The addition of foreign nanomaterials that can positively alter both selectivity and flux is probably the most promising mechanism for the development of the next generation breakthroughs in membrane technology. The incorporation of nanomaterials offer major advantages by providing specific membrane morphologies and the same time they can be the nucleus of additional physical-chemical interactions with the solute, thus providing higher selectivity as well as flux.

Nanocarbon membranes can be designed to enhance hydrophobicity, ion exchange, partition coefficient and other important transport properties. The combination of polymeric matrix and a nanomaterial needs to be optimized for a given application. In case of filtration or size selective applications, the nanomaterials can be implemented to alter pore size to improve the resolution in size cut off. The improvement in permeate flux will automatically lead to higher sensitivity and lower detection limit. This can be

accomplished by incorporating a nanomaterial that provides the optimum chemical-physical interactions with the analyte. The incorporation of carbon nanotubes in pervaporation and MD presented before are good examples. A variety of materials such as nanocarbons, zeolites, nanosilica are a few of the excellent candidates for this type of applications. These nanomaterials may also be functionalized with different functionalities that will provide further enhancement in flux as well as selectivity. The permutation and combinations of diverse types of membranes along with the available nanomaterials point towards some of utmost exciting possibilities in the future. An assessment of permeability and selectivity has shown asymptotic limitations on the separation capability of pure polymeric membranes. Efforts at improving these have looked at the development of novel materials as well as the modification of their structure and morphology. Recent interest has been focused on developing strategies for incorporation of nanomaterials [12] such as carbon nanotubes, zeolites, carbon black, gold in the bulk membrane matrix or on the surface.

Typically, the rate of mass transport through the membrane, Q, is controlled by the diffusion of solute can be estimated under steady-state conditions by use of the following equation :

$$Q = BAD(\Delta P)C_w / b \tag{1.9}$$

where, A is the surface area of the membrane, D is the diffusion coefficient in the membrane material, is the vapor pressure (or concentration) gradient, b is the thickness of the membrane, B is a geometric factor defined by the porosity of the membrane and is the inlet concentration. The presence of nanomaterials can affect several of these parameters; B and D are altered by the presence of the nanoparticles, while the partition coefficient is affected by the physical/chemical properties of the nanomaterials while their high surface area can facilitate greater flux. Therefore, an important consideration associated with the incorporation of nanomaterials in the membranes are their chemical properties, size distribution, agglomeration, interaction with the membrane matrix, effect on porosity, surface area and morphology. Additionally, such nanomaterials can be effective sorbents. Together these can enhance the selective partitioning as well as the permeation of the solute of interest.

A common approach to the fabrication of nanostructured nanocarbon membrane involves adding the filler material to a polymer solution followed by film casting or spinning and is referred to as the mixed matrix membrane (MMM) [22]. Good polymer-filler adhesion and uniform dispersion allows the formation of uniform membranes of submicron thickness. Such membranes possess some unique properties that benefit from the polymer as well as the nanofillers. Due to their small sizes, the nanoparticles can be implemented within micron or submicron thick films to serve as high flux barriers. An example is the fabrication of a polymeric layer tightly packed with nanomaterials like zeolite or CNTs to form a dense mixed matrix region. Incorporation of nanocarbons within polymeric membranes have been studied to increase permeate flux in extraction and pervaporation [23]. Dense arrays of aligned MWCNTs can potentially be used for

solute transport though the tube pores [24]. These exceptionally high transport rates as demonstrated by the CNTs was attributed to the specific pore size of the nanotubes, molecular smoothness of the surface and hydrophobicity and has been proposed as means for desalination via reverse osmosis [25]. Additionally, ability to tailor surface properties by chemical and biochemical functionalization of a specific nanomaterial is an attractive route for membrane development. Similarly they can be incorporated in porous structures where they alter the shape, size selective nature and allow molecular sieving. Nanocarbon membranes with incorporated nanocarbons are beginning to find applications in various fields such as extraction [26], pervaporation [27], and reverse osmosis [28]. Overall, nano structured membranes represent a versatile class of membranes that could have tremendous potential in a variety of separation applications for a wide range of analytes in diverse matrices ranging from environmental to biological. The combination of excellent adsorptive properties and tailor made nano carbons allows enhanced selectivity and permeation (Figure 1.5) of select analytes. Nanomembranes have been synthesized as porous as well as nonporous structures. The synthesis approached has varied from mixed matrix membranes to modification of existing membranes, and some of the common fillers have been variety of nanocarbons. The applications reported so far range from sampling devices to hollow fiber membranes for automated analysis by direct interfacing with instruments. The application of nanocarbon membranes is just in its nascent stages and it is anticipated that they have a bright future for industrial scale separations as well as analytical applications.

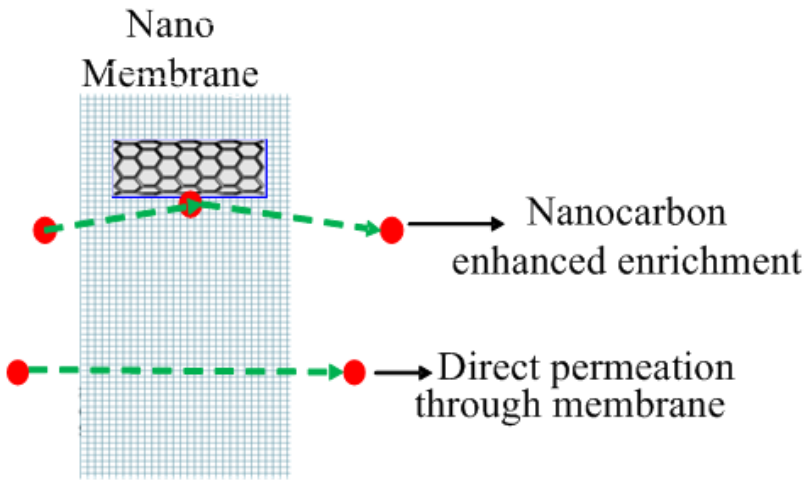

Figure 1.5 Permeation across Nanocarbon Membrane.

1.6 Objectives

The objective of this research was the exploration of carbon nanotube immobilized membrane (CNIM) for performance enhancement in two lead membrane separation processes, namely, analytical membrane extraction and membrane distillation. A state of the art of the implementation of carbon nanotube membranes on polar membranes for extraction of emerging polar analytes is addressed. Subsequent investigation and experimental studies were performed on functionalized carbon nanotube membranes (CNIM-f) for sweep gas membrane distillation (SGMD) and direct contact membrane distillation (DCMD) for desalination applications. With respect to the conventional membrane distillation membrane, the CNIM-f membrane demonstrated several appealing properties, which aided in improving the overall DCMD performance. Besides showing noteworthy enhancement in permeate flux, the CNIM-f membrane also exhibited long-term stability without any potential salt leakage. Further investigations were carried out utilizing emerging nanocarbons; namely, detonation nanodiamonds (DND) for

immobilizing membranes for SGMD and DCMD applications. This work is presented in six parts.

Part 1 Carbon Nanotube Immobilized Polar membranes for extraction of polar pesticides and non polar poly aromatic hydrocarbons

Membrane Extraction (ME) was investigated utilizing a solid polar membrane, namely nafion. This technique was aimed at exploring the possibility of immobilizing pristine as well as functionalized carbon nanotubes on a polar substrate for extraction of a wide range of emerging water contaminants including polar pesticides and non polar poly aromatic hydrocarbons.

Part 2 Enhanced Desalination Using Carboxylated Carbon Nanotube Immobilized Membranes

Desalination is the process by which high levels of salts are successfully removed from water allowing it to be used as pure drinking water. Functionalized Carbon nanotube membranes were fabricated and were investigated utilizing sweep gas membrane distillation technique as a means to improve desalination efficiency as compared to traditional membrane distillation. It was demonstrated that functionalized CNT immobilized membranes (CNIM-f) enhanced the vapor flux dramatically as compared to the standard membranes.

Part 3 Nanodiamond Immobilized Membranes for Enhanced Desalination via Membrane Distillation

In this study, the immobilization of DNDs within a hydrophobic membrane for membrane distillation desalination applications was investigated. Embedding only a minimal quantity (approximately 2%) of the nanocarbon, favorably altered the water vapor-membrane interactions to enhance water vapor permeability while preventing liquid penetration into the membrane pores thereby enhancing overall water vapor flux for the DND immobilized membrane.

Part 4 Flux Enhancement in Direct Contact Membrane Distillation (DCMD) by Implementing Carboxylated Carbon Nanotube Immobilized Membranes

With this work, the carboxylated carbon nanotube membrane was employed in direct contact membrane distillation mode for desalination. The performance of the newly fabricated membrane demonstrated superior performances over unmodified membrane with superior water vapor flux.

Part 5 Fabrication and Characterization of Hydrophobic Carbon Nanotube Membrane for Direct Contact Membrane Distillation (DCMD) Desalination

Hydrophobic octadecylamine CNT functionalized immobilized membrane was investigated for DCMD desalination applications. It was demonstrated that by and large,

the hydrophobic functionalized carbon nanotube membrane showed highest vapor flux enhancement as compared to conventional membranes.

CHAPTER 2

CARBON NANOTUBE IMMOBILIZED POLAR MEMBRANE FOR ENHANCED EXTRACTION OF POLAR ANALYTES

2.1 Introduction

The objective of this work [29] was to explore the effect of CNT incorporation and immobilization on a dense (or nonporous) membrane, and then on a polar substrate, and conclusively to investigate if such approach would dramatically improve its performance leading to enhanced enrichment factor and extraction efficiency for emerging polar as well as nonpolar water contaminants.

Recent years, have witnessed much interest in analytical applications of membrane extraction [30-32]. In a typical membrane separation, two phases come in contact without direct mixing, and the process can be made continuous. Membranes have also been used in diverse micro-scale extractions and hollow fiber membrane extractions for a variety of non-polar, polar and ionic analytes [30]. Of particular interest has been polar analytes that have ranged from pesticides, haloacetic acids to pharmaceuticals [33-37]. These have been extracted using polar membranes as well as supported liquid membranes. The former involves the use of polar materials such as polyurethane and nafion, while the latter uses an extractant immobilized in the membrane pores. Typical membranes represent a compromise between flux and selectivity, the ones with high selectivity tends to have lower permeability and vice versa. Recently the incorporation of CNTs in membrane structures have been reported [38-39], which offers several advantages and alternate mechanisms for solute transport. The physico-chemical properties of CNTs are known to play important roles in membrane processes, where the

nanotubes have served as channels for mass transport of water vapors and gases, and the high flux has been attributed to the atomic-scale smoothness of the CNT walls as well as molecular ordering inside the nanopores. Since CNTs act as both molecular transporters and sorbents, they can increase the permeability of a substance through a membrane as well as increase its selectivity. Since the CNTs are excellent sorbents, it is possible to implement them in multiple ways to enhance membrane separation. While it has been successfully immobilized in membrane pores to alter solute transport through pores, it is conceivable that just immobilizing them on a polar membrane surface will also alter transport behavior. Moreover, so far it has only been reported the immobilization of the nonpolar CNTs on non-polar membranes, but their effect on polar materials is yet to be studied.

2.2 Experimental

All chemicals and solvents used in the experiment were of analytical grade. Model compounds namely Atrazine, 1,2 Diphenylhydrazine, Pentachlorophenol, Anthracene, Naphthalene were purchased from Supelco (Supelco Park, PZ, USA). Nafion hollow fiber (0.533mm o.d x 0.356mm i.d) manufactured by Dupont, Wilmington, DE, USA was obtained from Permapure, Toms River, NJ, USA. The nafion membranes are a copolymer of tetrafluroethylene and perfluoro-3,6-dioxa-4-methyl-7-otene-sulfonic acid, and are highly polar. MWCNT (Multiwalled Carbon Nanotube) were obtained from Cheap Tubes. Inc. HPLC grade acetonitrile (Fisher Scientific, NJ, USA) was used as mobile phase in HPLC analysis and Deionized (DI) water was obtained from Millipore Gradient A10 water purification system (Millipore CO., Bedford, MA,

USA).

The membrane used here comprised of Nafion^{TM} (0.533mm o.d x 0.356mm i.d) hollow fiber, which is a copolymer of tetrafluroethylene and perfluoro-3, 6-dioxa-4-methyl-7-otene-sulfonic acid. Nafion is known to be highly polar and is used in such applications. To produce the CNIM, 10mg of MWCNT or carboxylated nanotubes (MWCNT-COOH) and 0.1mg PVDF was dispersed in 15mL acetone and sonicated for 3 hours. The dispersion was forced into the hollow fiber using a syringe and the excess was washed off with acetone. Scanning electron microscopy (SEM) images of the CNIM were taken using an LEO 1530 VP (Carl Zeiss SMT AG Company, Oberkochen, Germany). The unmodified nafion membrane and the CNIM were cut into 0.5cm long pieces and coated with a carbon film prior to SEM analysis. FTIR analysis was carried out using a 510 Nicolet spectrophotometer and Thermal gravimetric analysis (TGA) was carried out using Perkin-Elmer Pyris 7 TGA system at a heating in N_2 at the rate of 10^{o}C/min from 30˚C to 800˚C.

The performance of nafion CNIM was assessed using hollow fiber based microscale membrane extraction and are shown in Figure 2.1. It is essentially liquid-liquid extraction across the membrane. Two 50 µl syringes (Hamilton, Reno, NV, USA) were pierced through the septum and were used to hold the membrane in place. One of the syringes was used to inject 50µl of organic extractant and the other to withdraw the extract. The membrane assembly was suspended in a bottle containing the analyte mixture and extraction was carried out at a stirring speed of 80 rpm for an hour using a Corning PC-353 Stirrer. IPA (iso propyl acetate) was the main extractant used for this

study. After the extraction, the acceptor was withdrawn and measured by the syringe and finally transferred into a vial for HPLC analysis.

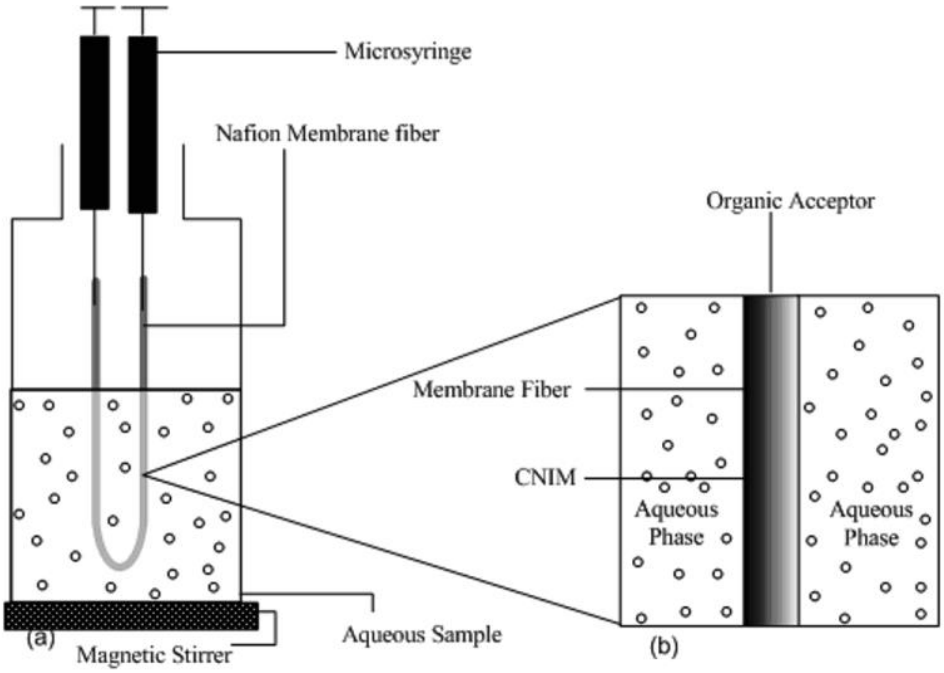

Figure 2.1 Schematic diagram of experimental set up of µ-scale membrane.

HPLC analysis was carried out with Hewlett-Packard 1050 equipped with Waters 486 tunable absorbance UV detector, and a 4.6 x 150 mm, 5 µm Zorbax column). Peak simple ver.3.29 (SRI Instruments, Torrance, CA) was used for chromatographic data acquisition.

2.3 Results and Discussion

The incorporation of CNTs in nafion immobilized membrane was characterized and confirmed by Scanning Electron Microscopy (SEM), FTIR and Optical spectrometry. The SEM images of parent Nafion, CNIM and CNIM-COOH are shown in Figure 2.2. The unmodified membrane is shown in Figure 2.2 a. The presence of CNTs made the membranes darker in colour. The CNT strands are clearly visible on the membrane surface, which were absent on the parent Nafion (Figure 2.2 b and c). The SEM images also show that the CNT incorporation was uniform. Figure 2.2 d shows the raman microscopic images of the parent hollow fiber and Figure 2.2 e shows the image of immobilization of CNT on parent nafion. The presence of CNTs was evident from the distinctly observed dark patches, which was absent in parent nafion membrane.

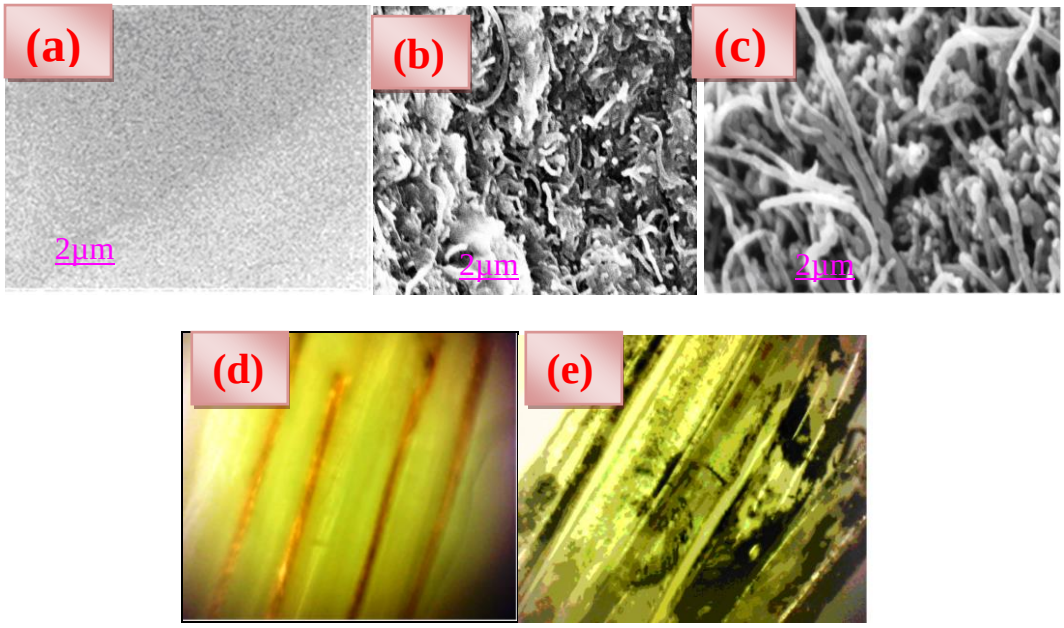

Figure 2.2 A) SEM images of surfaces of (a) Unmodified Nafion Membrane (b) CNIM (c) CNIM-COOH B) Confocal Raman Microscopic images (d) Unmodified membrane (e) CNIM.

FTIR was used to study the chemical characteristics of the membrane. The IR spectra of the parent nafion and CNIM are presented in Figure 2.3. In the spectra depicting parent membrane, there are two strong peaks at 1215cm^{-1} and 1319cm^{-1}. The absorbance peak at 1215cm^{-1} could be attributed to the asymmetrical C-F stretching band of the nafion perfluorosulfonic acid backbone and the peak at 1319cm^{-1} was assigned to the symmetrical C-F stretching bands of the same. Hence, both C-F absorbance bands appeared prominently. The absorbance peak at 1024cm^{-1} was assigned to S=O stretching bands. Two peaks at 2854cm^{-1} and 2999cm^{-1} were assigned to the asymmetrical and symmetrical C-H bands. Additional band at 3446cm^{-1} was attributed to the hydroxyl group of parent Nafion membrane. Introduction of CNTs in modified membrane produced new bands which appeared at around 1563cm^{-1} which could be attributed to the graphene structure and the termination of CNTs with COOH showed new bands at 1705cm^{-1} which were attributed to C=O stretching vibration of carboxyl group. Thus, based on the IR results it can be concluded that the CNTs, as well as CNT-COOH were successfully incorporated on the membrane surface [40].

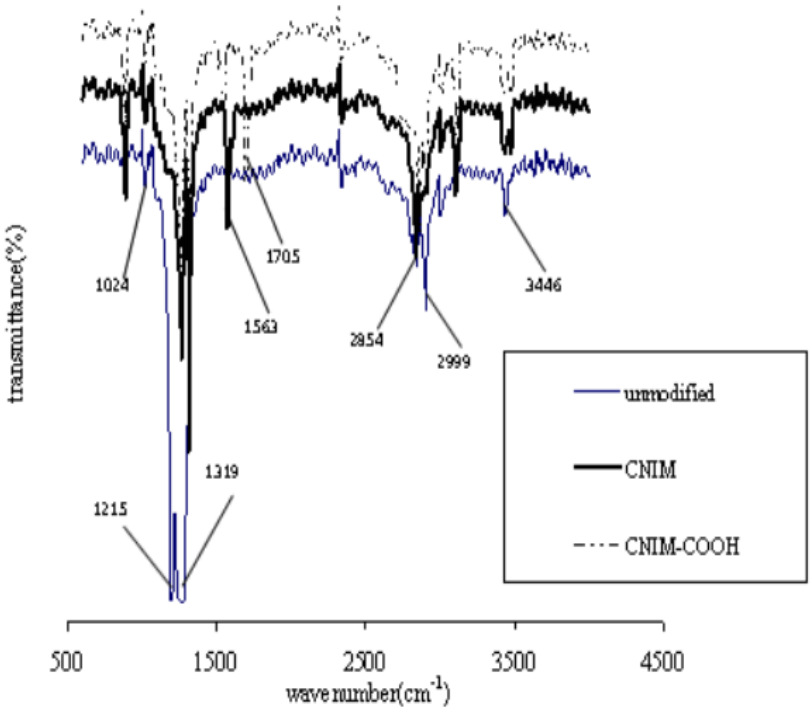

Figure 2.3 FTIR spectra of Unmodified Nafion Membrane, CNIM and CNIM-COOH.

2.4 Analytical Performance Enhancement in CNIM

Permeation (P) of analytes as well as solvents in the solid membrane is expressed as a solution-diffusion model according and Fick's law of diffusion, which may be expressed as:

$$P = BAP(\Delta C)C_w / b \qquad (2.1)$$

where, A is the surface area of the membrane, P is the diffusion coefficient in the membrane material, ΔC is the concentration gradient, b is the thickness of the membrane, B is a geometric factor defined by the morphology of the membrane and C_w is the analyte concentration on the donor side. In a solution-diffusion model applicable to solid membranes, P= DS, where, S is solubility and D is diffusivity. The CNTs assist in diffusion by providing additional routes for mass transport. The strong sorbent characteristics enhance the overall S, for example the CNT surfaces provide weak (π-π) attachment sites for analyte molecules and also served as contact sites for two phases and subsequent liquid liquid extraction. In short, the presence of CNTs affects several of these parameters; B and D are altered by the presence of the smooth and frictionless surface of CNTs, while the partition coefficient is affected by the excellent sorbent characteristics of the CNTs and their high surface area increases the effective area.

In this research the effectiveness of the membranes were assessed in terms of enrichment factor which is defined as the ratio of analyte concentration in the final extract to that in the original water sample and is directly related to sensitivity and detection limit [41-44]. CNIM was evaluated by micro-scale membrane extraction via liquid-liquid extraction (μ-LLME). This is a two phase system where the solute is extracted from an aqueous solution into an organic extractant. Atrazine, Pentachloro phenol, 1,2 diphenyl hydrazine, anthracene and napthalene were used as test analytes to study the enrichment of this proposed phenomenon. The extractions were carried out with parent nafion membrane, CNIM and CNIM-COOH. The results are presented in Table 2.1. All measurements had relative standard deviations between 1-6%.

Table 2.1 Membrane Efficiency from Micro-scale Membrane Extraction of Water Samples [a)]

Analytes	Plain		CNIM		CNIM-COOH		Enhancement %	
	EF	EE%	EF	EE%	EF	EE%	CNIM	CNIM-COOH
Atrazine	118	1.9	205	3.9	192	3	74	63
PCP	108.8	1.7	151	2.8	110	1.9	39	1.0
1,2 DPH	196.2	3.2	282	5.4	222	3.9	44	13
Anthracene	146	2.4	192	3.7	180	3	32	23
Naphthalene	94	2	180	3.4	180	3	92	92

a) Experimental conditions were as follows: initial isopropyl acetate volume 50 µL; sample volume 200 mL; stirring rate 80 rpm.

For all test compounds studied here, the CNIM yielded higher EF compared to the parent nafion. For non-polar naphthalene and anthracene, EF improved significantly somewhere between 32-92%, while for the polar compounds the enhancement was higher. EF of highly polar compounds like atrazine was enhanced by 63 to 74% by CNT and CNT-COOH, respectively, while EF for pentachlorophenol and 1,2DPH increased by 39 and 44% respectively using CNT. In previous studies [38] where CNIM was synthesized using hydrophobic polypropylene, the EF for atrazine was only 2.6 as compared to 205 and 191.85 for the current study with CNT and CNIM-COOH immobilized on Nafion^{TM} backbone. This is a major enhancement in performance based on using a polar base membrane. This was attributed to the fact that the parent nafion backbone contained fluorocarbon chains terminating in sulfonic acid groups, which exhibited high permeability for primary and secondary amines.

In addition to the conventional membrane extraction where the sample and extractant contacted across the dense membrane, the CNT introduction provided enhanced solute transport. As shown in Figure 2.4, the solvent and the analytes first adsorbed on CNT surface where extraction took place. The presence of CNTs increased surface area, the overall partition coefficients and the solute in contact with the CNTs readily desorbed into the acceptor phase. Additionally, the Nafion^{TM} substrate is a polar membrane and hence it would allow the permeability of water sample through it. The presence of CNTs provided a barrier for preventing water permeation. The overall effects of these factors were to enhance the EF as well as EE%.

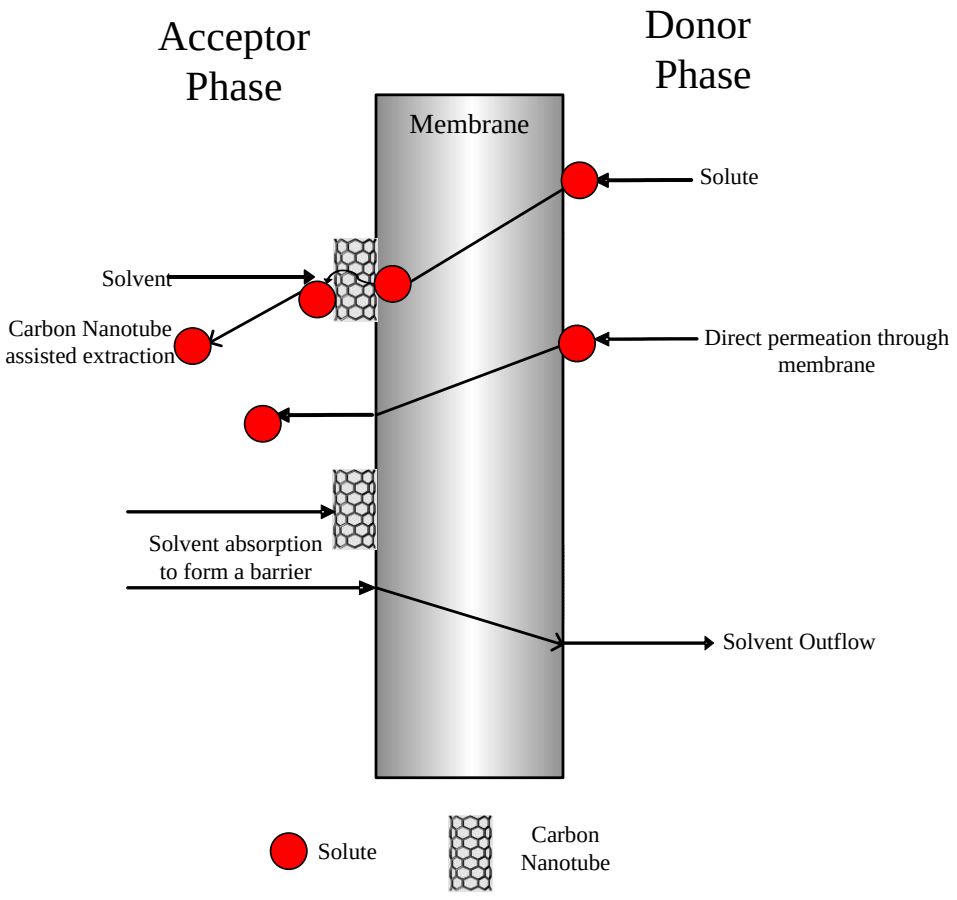

Figure 2.4 Mechanism of Microextraction in presence of CNTs.

The carboxylic group on the CNT surface did not provide additional advantage, although enhanced performance over the Nafion^{TM} membrane was observed, it was not as good as the pure CNT.

2.5 Solvent Retention in CNIM

During membrane extraction, while the analytes flow into the extractant, the extractant has the tendency to flow out as well. The permeation of extractant is undesirable because it leads to mixing of the two phases, and some solutes are also lost along with this, thus reducing extraction performance. The solvent can be lost through the membrane by permeation and by solubilizing in water. Therefore several factors including polarity, ability to hydrogen bond and molecular size come into play. In this study, the retention of seven different solvents with varying polarity and water solubility was tested by enclosing a few microliters of the solvent in the membrane lumen and following their out migration over time. This was done by measuring solvent volume before and after the extraction. All measurements were made in three replicates and the relative standard deviations were between 2-6%. Their octanol water coefficients and water solubility are presented in Table 2.2. In all cases, the presence of CNTs dramatically enhanced solvent retention. Solvents such as methanol, ethanol, acetonitrile, which are highly polar and water miscible suffered extensive loss, and were easily lost through the polar nafion.

Table 2.2 Solvent loss in presence of CNTs

Solvents	log Kw [b]	Solubility in water	Solvent loss (%)		
			Plain	CNIM	
				CNIM	CNIM-COOH
Methanol	-0.77	Miscible	100	86	82
Ethanol	-0.31	Miscible	96	90	80
ACN	-0.34	Miscible	100	92	92
IPA	1.03	30.9gm/L	34	24	29
BA	1.78	8.4g/L	55	40	63
Hexane	3.9	9.5mg/L	77	56	64
n-Decane	5.01	Immiscible	75	54	60

a) Experimental conditions were as follows: initial solvent volume, 50 µL; Sample solution, 200 mL; Retention time: 30min; No stirring; [b] K_{ow} is octanol–water coefficient; ACN – Acetonitrile; IPA- Isopropyl Acetate; BA- Butyl Acetate

Isopropyl Acetate (IPA) which was less polar than the above solvents but more polar than hexane, Butyl Acetate (BA) and n-decane showed the least solvent loss in nafion and the CNIM. Additionally, iso propyl acetate is a relatively more viscous solvent (0.6 mPa·s) as compared to hexane (0.294 mPa·s), which reduced its mass transport rate through the membrane. The retention of polar solvents (methanol, ethanol and acetonitrile) increased 6.4-18%, while those for the relatively less polar solvents by 4-29%. The presence of CNTs had multiple effects. Being non polar, it provided a barrier to the transmission of polar molecules. On the other hand, being a good sorbent, the solvent concentration on the CNTs probably increased to the point that it reduced the concentration gradient across the membrane thus reducing permeation. The CNIM and CNIM-COOH showed different effects. For example,

compared to unmodified nafion, the presence of CNTs showed enhancement of up to around 29% where as CNIM-COOH showed enhancement up to 20%.

Based on its low solvent loss and midrange polarity, isopropyl acetate was selected as the extraction solvent, its loss was investigated as a function of extraction time, and this is shown in Figure 2.5. The donor volume and the stirring rate were same as for the previous data. As seen from the graph, for the first 5 minutes, both membranes showed similar behavior, however solvent loss increased at a faster rate in the unmodified membrane. The solvent loss at 30 minutes for unmodified nafion was 34% while in that of CNIM was 24%. Solvent loss was more evident when extraction time reached 60 minutes, when it was observed that the loss in plain nafion was 36% compared to 24% for CNIM.

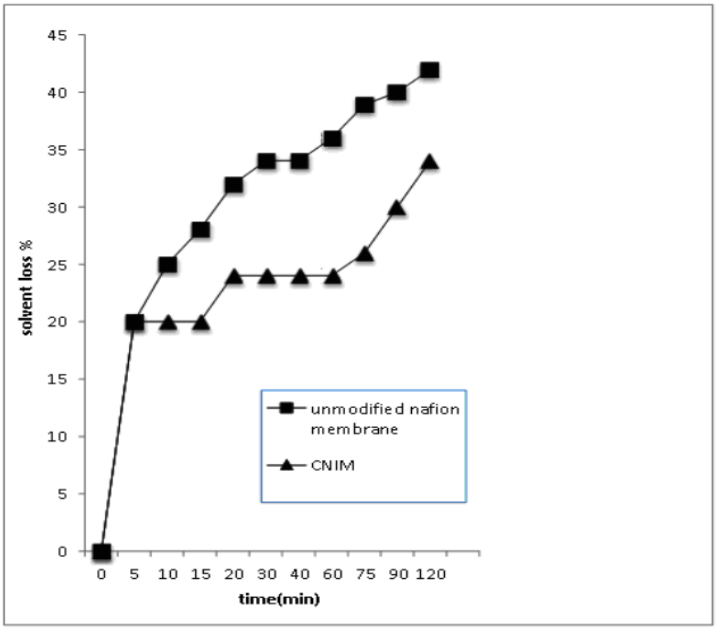

Figure 2.5 Outflow of IPA (Isopropyl Acetate) as a function of time.

2.6 Conclusion

In this study, an immobilization of CNT on the surface of polar Nafion has been presented. The immobilized membrane was able to provide enhanced enrichment by using it to extract the polar pesticides and non polar polycyclic aromatic compounds from water samples by μ-ME technique. The CNTs served as sorption sites for extraction and led to an overall increase in extraction efficiency and enrichment factors. It was also found that the inclusion of CNTs led to the retention of extraction solvent. Overall, the presence of CNTs led to the enhancement of enrichment factors and retention of solvent for both the polar and nonpolar solvents. The carboxylation of the CNTs did not appear to increase enhancment over the raw CNTs, but it is conceivable that a polar membrane with appropriate surface modification with CNTs can provide a platform for potential enhancement in the extraction of polar compounds in membrane extraction.

CHAPTER 3

ENHANCED DESALINATION USING CARBOXYLATED CARBON NANOTUBE IMMOBILIZED MEMBRANES

3.1 Introduction

Water is an essential resource for ensuring human health, and the lack of suitable water to meet the daily needs for human consumption is a reality. The importance of water to life on earth can not be too highly stated. The lack of sufficient quantities of water suitable for human consumption is a growing problem and is recognized by agencies such as the World Health Organization (WHO) as the most serious threat to the health of global populations. As the shortage of clean water looms in the horizon, there is much interest in developing novel, cost effective desalination technology. While there are existing technologies that can remove these high salt levels in water, they are expensive and technically difficult to operate and maintain. These are also prone to failure due the corrosive effects of the salts. Currently the most commonly used process for seawater desalination is thermal distillation and reverse osmosis (RO) [45-50]. RO is a process by which water is deionized by using pressure. Because of the relatively high pressures (300-1000 psi) involved in RO; specialized equipment is needed, such as pressure vessels to contain the membranes and multi-stage pumps. Membrane distillation (MD) has emerged as an alternative to address some the issues related to those current technologies [51-53]. Here a hot salt solution such as sea or brackish water is passed through (or across) a hydrophobic membrane which acts as a physical barrier separating the warm solution from a cooler permeate. The permeation is driven by a vapor pressure gradient resulting from the temperature difference and solution composition gradients across the membrane. Typically, MD is carried out at 60-90ºC, which is significantly lower than

conventional distillation. Therefore, it has the potential to generate high quality drinking water using only low temperature heat sources such as waste heat from industrial processes and solar energy.

The main effort in optimal design involves the maximization of solute rejection and flux, which would make MD commercially viable. A key component in such a process is the membrane itself because it determines both flux and selectivity. Several membrane material based on polypropylene, Polyvinylidene fluoride (PVDF) and Teflon have been used in MD [53]. Some recent developments include surfaces made of zeolite, clay nanocomposites nanofiber, silane grafting and modification by hydrophobic porous alumina [54-56].

Carbon nanotube based membranes have been used in a variety of separation applications in various formats [57] that range from forward osmosis [58] to nanofiltration [59-61]. Recently it was demonstrated that immobilizing CNTs in different types of prefabricated membranes alter the solute-membrane interactions, which is one of the major physicochemical factors affecting the permeability and selectivity. Referred to as carbon nanotube immobilized membrane (CNIM), here the CNTs serve as a sorbent and provide an additional pathway for solute transport. These membranes have been used in nanofiltration, MD, solvent extraction and pervaporation, and have demonstrated superior performance [59].

An important consideration that is yet to be fully utilized in membrane separation is that CNTs can be effectively functionalized to alter its chemical properties, which could lead to specific interactions with solutes, or just a change in hydrophilicity. This has been demonstrated in nanofiltration applications [59]. The objective of this research

was to study if functionalization, in particular carboxylation will increase the interaction of nanotubes with the polar water vapor and result in improved desalination efficiency [62].

3.2 Experimental

The membrane modules for MD were constructed in a shell and tube format using ¼ inch polypropylene tubing (Figure 3.1). Ten, 16.6cm long hollow fiber strands were used in the module. Each module contained approximately 12.50 cm^2 of effective membrane contact area (based on internal surface). The ends were then sealed with epoxy to prevent leakage into the shell side. Vacuum was applied to one drain port to draw dry air through the other port, which created a higher pressure differential and provided a sweep air.

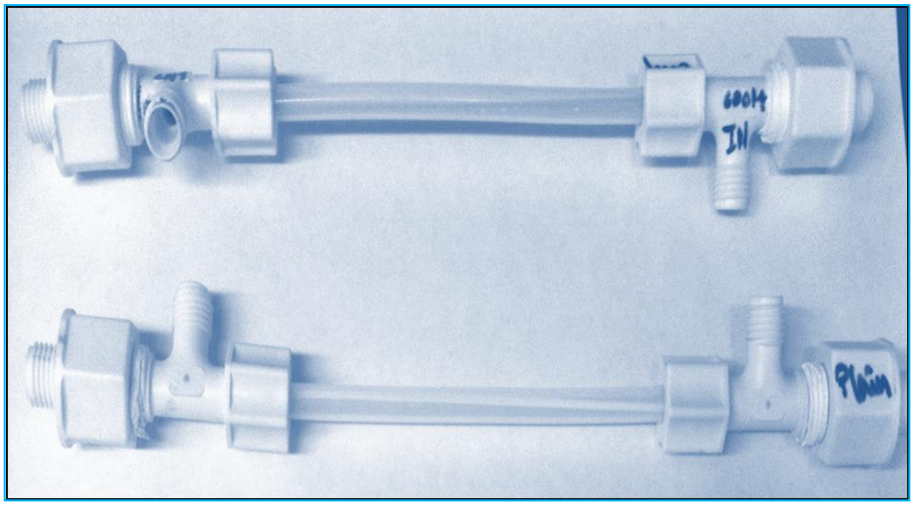

Figure 3.1 Hollow fiber membrane modules.

The synthesis of carboxylated CNTs (MWCNT-COOH) was carried out as follows. Pristine MWCNT was purchased from Cheap Tubes, Inc., Brattleboro, VT,

USA. As previously mentioned in Chapter 2 [29] CNT carboxylation was carried out in a Microwave Accelerated Reaction system (CEM Mars) fitted with internal temperature and pressure controls. Three hundred milligram of original MWCNTs was added to the reaction chamber together with 25ml 1:1 conc H_2SO_4 and HNO_3. The reaction was carried out at 120^o C for 40 min. After cooling, the product was vacuum filtered using a Teflon membrane with pore size (0.45µm), and the solid was dried in a vacuum oven at 70^oC for 5 hours. This led to the formation of carboxylated MWCNTs (MWCNT-COOH) which was characterized by FTIR which confirmed the presence of carboxyl groups. The results are not presented here for brevity.

The CNIM with pure CNT (referred to as CNIM) and functionalized CNT (referred to as CNIM-f) were prepared using Celgard type X30-240 (Celgard, LLC, and Charlotte, NC, USA) hollow fiber with pore size (0.04 µm) as the starting material. For the preparation of CNIM and CNIM-f, each of 10 mg of MWCNT and MWCNT-COOH were dispersed in a solution containing 0.1 mg of polyvinylidene fluoride in 15 ml of acetone by sonicating for three hours. The Polyvinylidene fluoride (PVDF) - nanotube dispersion was forced under controlled vacuum into the bore of the polypropylene hollow fiber membrane. The PVDF served as glue that held the CNTs in place and led to its encapsulation within the membrane, and this may also affect the membrane performance. The membrane was flushed with acetone to remove excess nanotubes. The original polypropylene membrane was sonicated in PVDF solution in acetone without the CNTs, and this served as the control. The morphology of CNIM and CNIM-f were studied using scanning electron microscopy (SEM, Model LEO 1530), and Thermo gravimetric analysis (TGA) was performed using a Perkin Elmer Pyris 7 TGA instrument to study the

thermal stability of the membrane. Differential scanning calorimetry (DSC) was also carried out using a Universal V4.5A TA instrument to observe the alterations in thermal properties.

The schematic of experimental system is shown in Figure 3.2. The feed used in these experiments contained 3.4 wt% NaCl solutions (Sigma Aldrich). This was pumped through the module using a Master flex 7519-10 peristaltic pump. The preheated hot feed solution travelled through a heat exchanger which was used to maintain the desired temperature through out the experiment. Dry air was passed into the shell side and the permeate was collected in a trap. Air flow was maintained at 1 liter min^{-1}. The ionic strength of the original solution, the permeate and the concentrate were measured using a Jenway Electrode Conductivity Meter 4310. Each experiment was repeated three times to check the reproducibility and relative standard deviation was less than 1%.

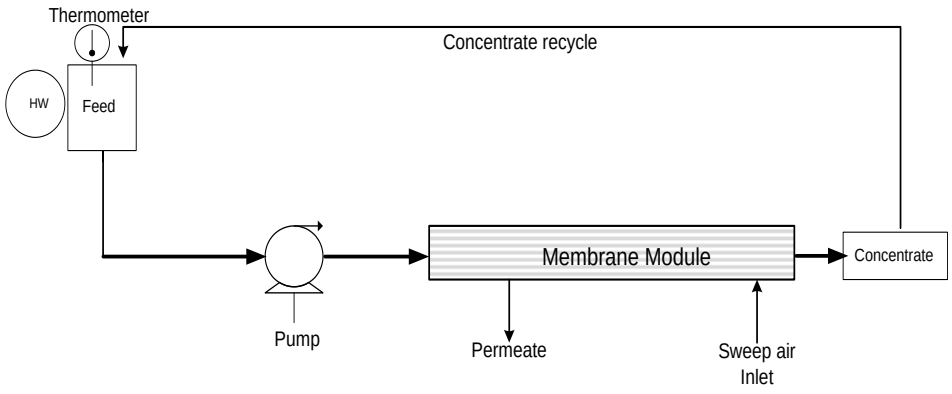

Figure 3.2 Schematic diagram of the experimental system.

3.3 Results and Discussion

Scanning electron micrographs of the unmodified membrane and CNIM-f are shown in Figures 3.3a and b. The incorporation of the carboxylated CNTs is clearly evident in

Figure 3.3b. Additionally, Figure 3.3c depicts the intactness of CNT-COOH within the membranes after 90 days of continuous usage. The TGA curve is shown in Figure 3.4a. As observed, the thermal degradation of unmodified polypropylene membrane started at around 260^{o}C. However, in line with previous observations, the presence of CNT-COOH increased the degradation temperature by 40^{o}C. This implies that the CNT-COOH was highly stable and enhanced the thermal stability of the membrane. This is an important factor for MD, where the elevated temperatures can be used for desalination [22]. This data was also supported by differential scanning calorimetry (DSC) and is presented in Figure 3.4 b. No specific degradation or alterations was observed in the CNIM-f.

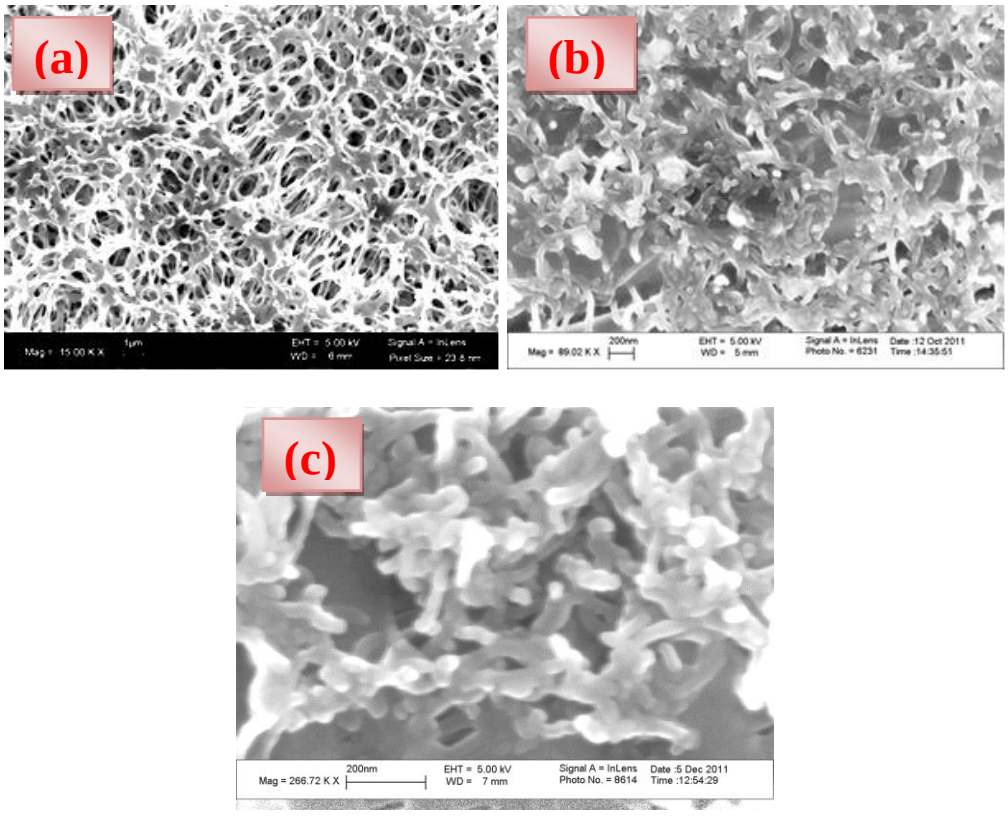

Figure 3.3 SEM images of the (a) unmodified Membrane (b) CNIM-f (c) CNIM-f after 90 days of operation.

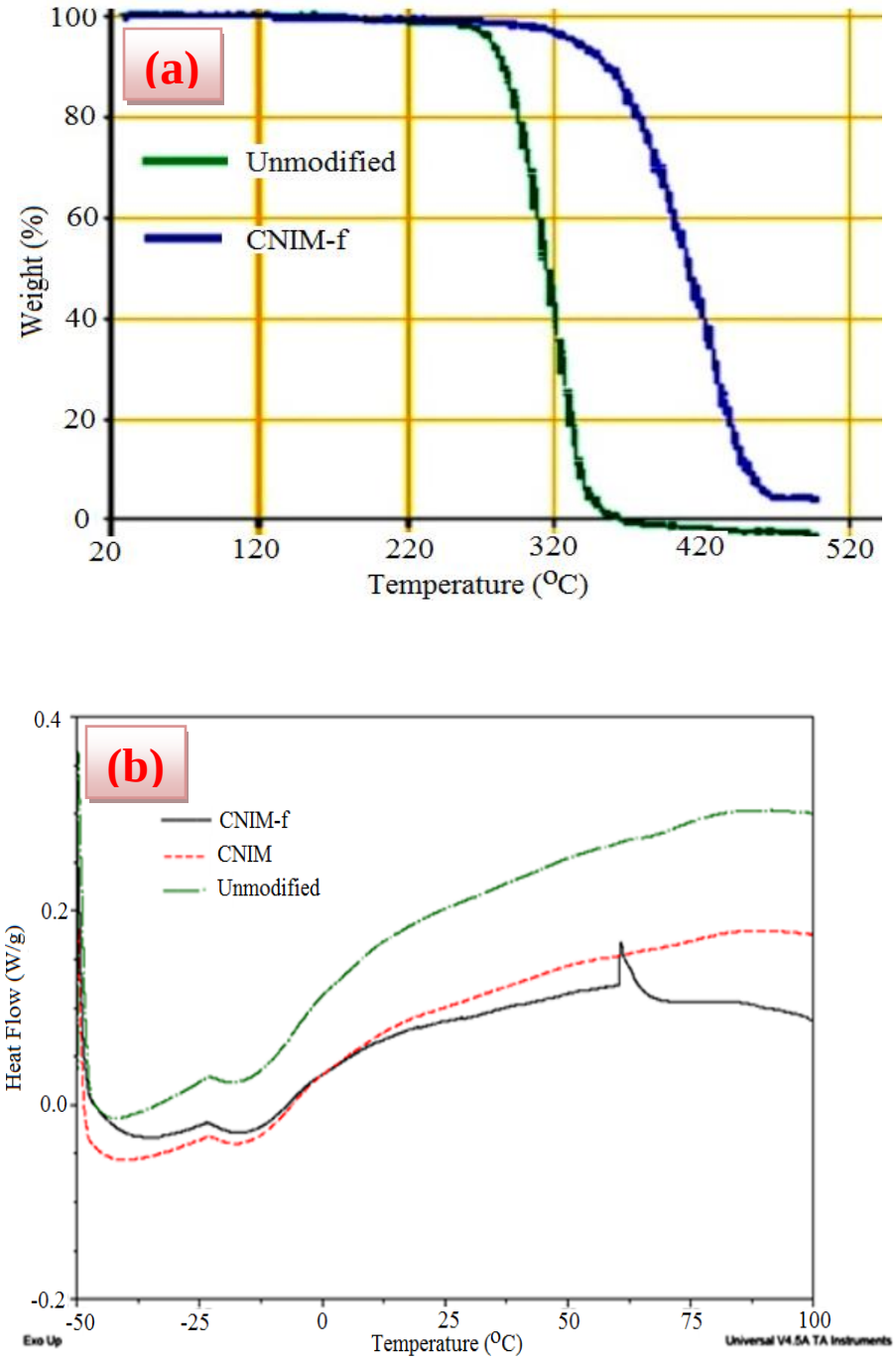

Figure 3.4 a) Thermal gravitational analysis of unmodified membrane and CNIM-f (b) Differential Scanning Colorimetry of all three membrane types.

The CNIM and CNIM-f were tested for SGMD. The water vapor flux, J_w, across the membrane can be expressed as:

$$J_w = \frac{w_p}{t.A} \tag{3.1}$$

where, w_p is the total mass of permeate, t is the permeate collection time and A is the membrane surface area. Also, J_w can be denoted as:

$$J_w = k(C_f - C_p) \tag{3.2}$$

where, k is the mass transfer coefficient, C_f and C_P is the water vapor concentration in feed and permeate side. Usually C_p is close to zero, since we utilize dry air as sweep gas. So overall mass transfer coefficient was calculated as:

$$k = \frac{J_w}{C_f} \tag{3.3}$$

As can be observed in Figure 3.5, increasing temperature increased flux for all three-membrane types. Flux at 70^{o}C using the either CNIM or CNIM-f was higher than what was obtained by the unmodified membrane. Maximum flux reached up to 19.2 kg/m^{2}h for CNIIM-f membrane and 15.6 kg/m^{2}h using CNIM. The enhanced performance on CNIM as compared to unmodified membrane has already been studied previously [25]. However, what is unique here is that, the permeate flux was the highest for CNIM-f membrane.

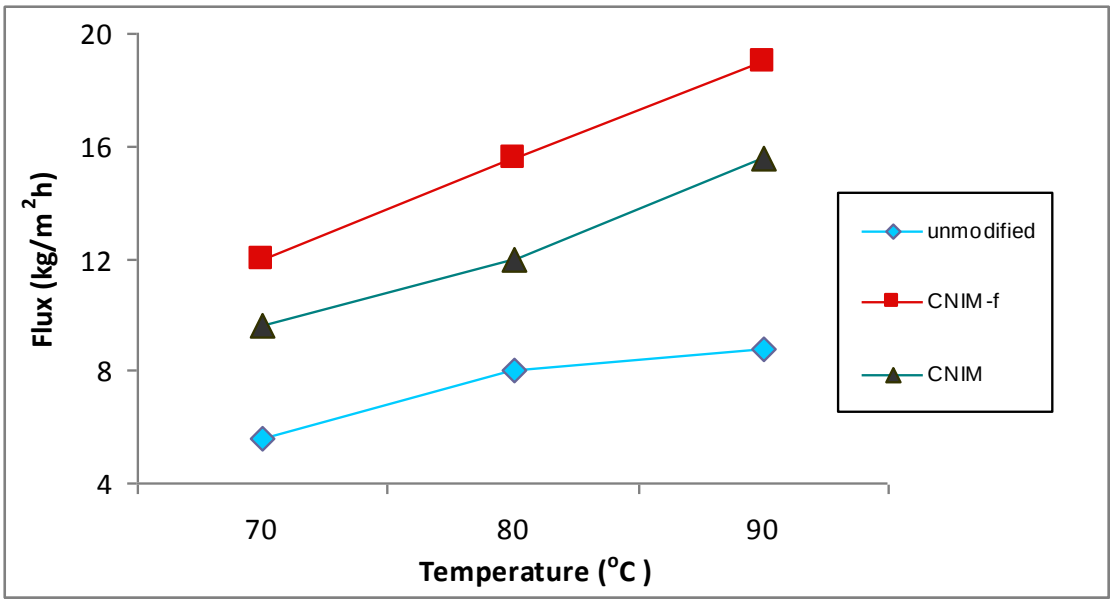

Figure 3.5 Effect of temperature on permeate flux at a feed flow rate of 20 ml min^{-1}.

Desalination as a function of flow rate is shown in Figure 3.6. It can be observed that increasing flow rate increased permeate flux. As observed, compared to unmodified membrane, CNIM and CNIM-f demonstrated higher flux at all flow rates. At elevated flow rate, there was reduced boundary layer and adsorption-desorption processes were faster.

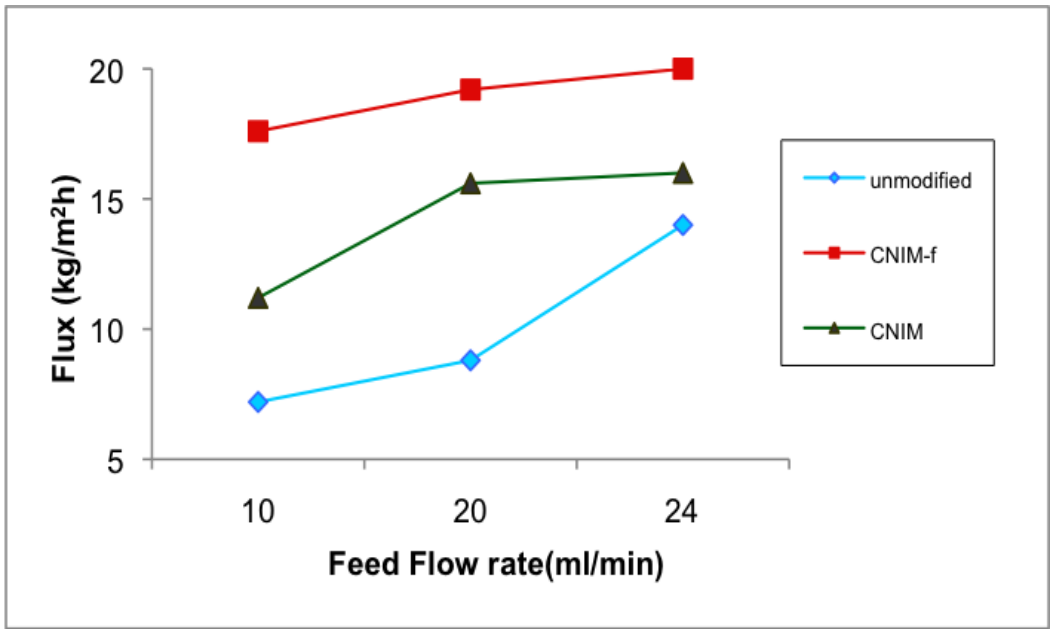

Figure 3.6 Effect of flow rate on permeate flux at feed temperature 90^{o}C.

Figure 3.7 depicts the effect of varying of feed concentration on permeate flux. It is well known that concentration polarization is more important at higher feed concentration. At higher feed concentration, a more significant boundary layer develops next to the membrane interface and this reduces driving force of mass transfer. This leads to the decrease in permeate flux in case of unmodified membrane modules. On the other hand, in case of CNIM, and CNIM-f, the flux remained unchanged. The presence of CNTs increased the surface roughness that prevented the formation of stable boundary layers. As observed from Figure 3.7, for CNIM-f, the flux remained constant with increasing salt concentration, reaching up to 19.2 kg/m^{2}h.

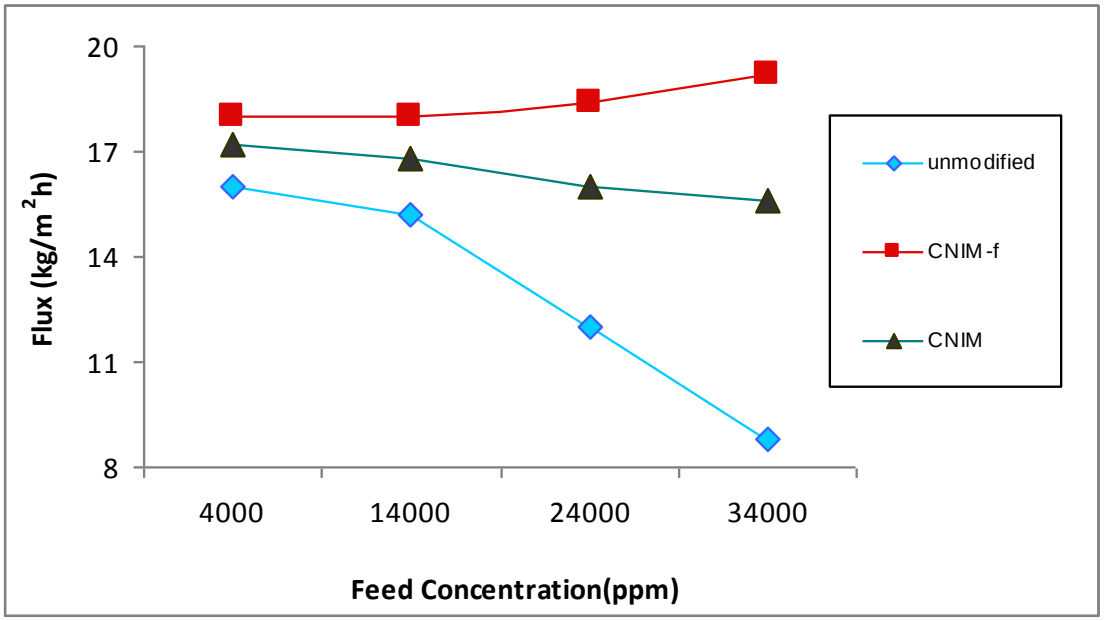

Figure 3.7 Effect of feed concentration on permeate flux at a feed flow rate of 20 ml min^{-1}, 90^{o}C.

Incorporation of various weights of CNT loadings/cm^2 of membrane area was also investigated. An optimum value of 0.005 mg per centimeter square loadings of MWCNT was required to enhance the overall percent removal and flux. A further increase of CNT loading (0.008 mg per centimeter square) did not showed any further enhancement. It was estimated that significantly higher MWCNT amount would block the pores of the hydrophobic membrane, thereby reducing flux and removal efficiency.

Additionally, as observed from Table 3.1, the mass transfer coefficients enhancements were found to be significantly higher for CNIM-f as compared to the unmodified membrane. Enhancement for CNIM ranged between 50%-77%. However, for CNIM-f, enhancement ranged from 95%-116%. Table 3.2 indicates the effect of feed flow rate on mass transfer coefficients. As observed, the overall mass transfer coefficient was enhanced by presence of CNIM-f. Interestingly, the enhancement in mass transfer

coefficient was higher at a low flow rate. At a flow rate of 10 mL/min, the mass transfer coefficient of the CNIM-f was 145% higher than the unmodified membrane, whereas for CNIM enhancement was just 56% but the corresponding values dropped to 27% and 59% when inlet feed flow rate was 24ml/min. In general, the presence of the CNT-COOH led to enhanced permeability through the membrane, and the CNIM-f showed a significantly higher overall mass transfer coefficient. An important observation from Figure 3.8 is that, whereas an increase in feed concentration decreased k for the unmodified membrane, it but remained almost constant and showed negligible decease for CNIM and CNIM-f. At 34000mg L^{-1}, the mass transfer coefficient was more than double for CNIM-f than the plain membrane, which was significantly higher than what was previously as reported [25].

Table 3.1 Mass Transfer Coefficient and Enhancement % at Various Feed Temperature at Feed Flow Rate 20ml/min

	Mass Transfer Coefficient X 10^7 ($kg/m^2.s.Pa$)			**Enhancement (%)**	
Temp(^oC)	**Unmodified**	**CNIM**	**CNIM-f**	**CNIM**	**CNIM-f**
70	**0.499**	**0.856**	**1.07**	**72**	**114**
80	**0.469**	**0.704**	**0.915**	**50**	**95**
90	**0.349**	**0.618**	**0.753**	**77**	**116**

Table 3.2 Mass Transfer Coefficient and Enhancement % at Various Feed Flow Rate at Feed Temperature 90^{o}C

	Mass Transfer Coefficient X 10^7 (kg/m^2.s.Pa)			Enhancement (%)	
Flow rate(ml/min)	**Unmodified**	**CNIM**	**CNIM-f**	**CNIM**	**CNIM-f**
10	**0.285**	**0.444**	**0.697**	**56**	**145**
20	**0.349**	**0.618**	**0.753**	**77**	**116**
24	**0.5**	**0.634**	**0.793**	**27**	**59**

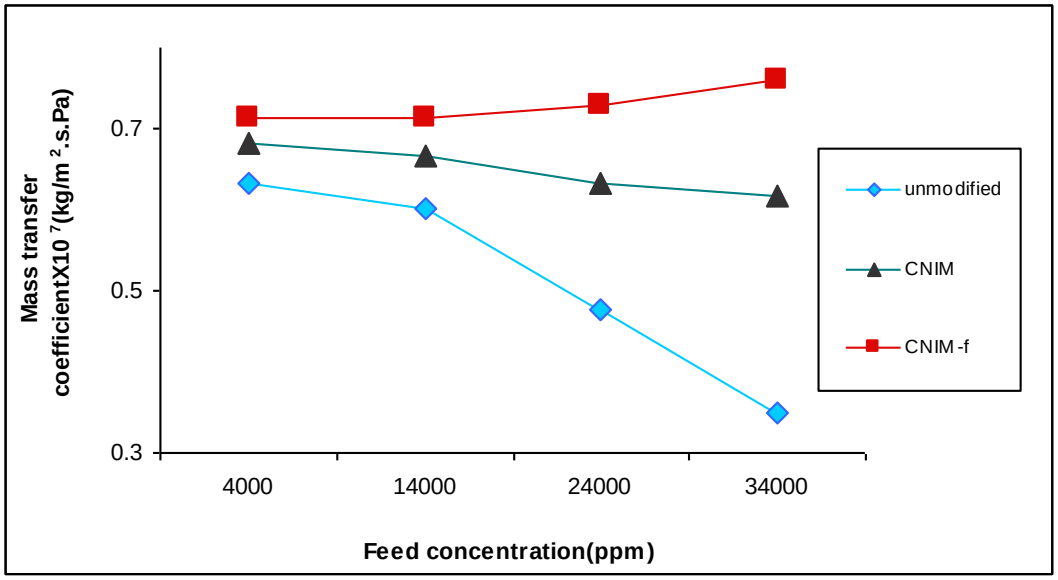

Figure 3.8 Effect of feed concentration on Mass transfer coefficient at a feed flow rate of 20 ml min^{-1} , 90^{o}C.

3.4 Salt Breakthrough and Stability of CNIM and CNIM-f

There was no observable salt breakthrough in any of the experiments, and the permeate showed low conductivity of 1 to 2.5μS/cm at 20^0C, implying that the water had over 99.9% purity. The stability of the membrane, especially the ability to retain the CNT coating on the surface was tested for long-term operation. A test was carried out for ninety days and there was no observable decrease in flux over this period of time using either CNIM or CNIM-f. This is shown in Figure 3.9. The SEM images of CNIM-f after 90 days of operation also did not show any visible signs of CNT erosion or damage.

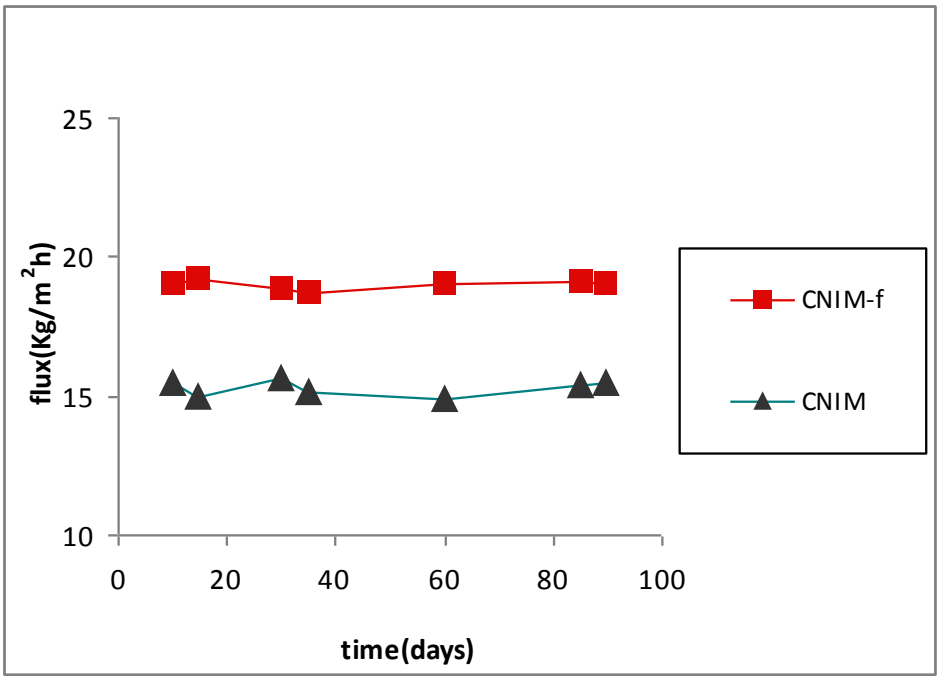

Figure 3.9 Operational period stability study of CNIM, CNIM-f membrane.

3.5 Proposed Mechanism

Due to a combination of factors mentioned above, significantly higher flux was observed for CNIM and CNIM-f as compared to conventional membrane. This was attributed to the fact that the CNTs serves as sorbent sites for vapor transport while rejecting the liquid

water. The carboxylated CNTs are polar and they provided higher sorption for the water vapors than unfunctionalized CNTs, thus enhancing flux **(**Figure 3.10). Under normal circumstances one would expect the hydrophilic CNT-COOH to decrease the overall hydrophobicity of the membrane and also interact with the sodium ions. Therefore, one would expect the performance of CNIM-f to be lower than CNIM. However, since PVDF dispersion was used to immobilize the CNT-COOH, the former encapsulated the latter, which prevented water as well as Na^+ ions from reaching the nanotubes. On the other hand, the water vapors that permeated through the PVDF surface was able to partition on the CNT-f and effectively permeate through the membrane.

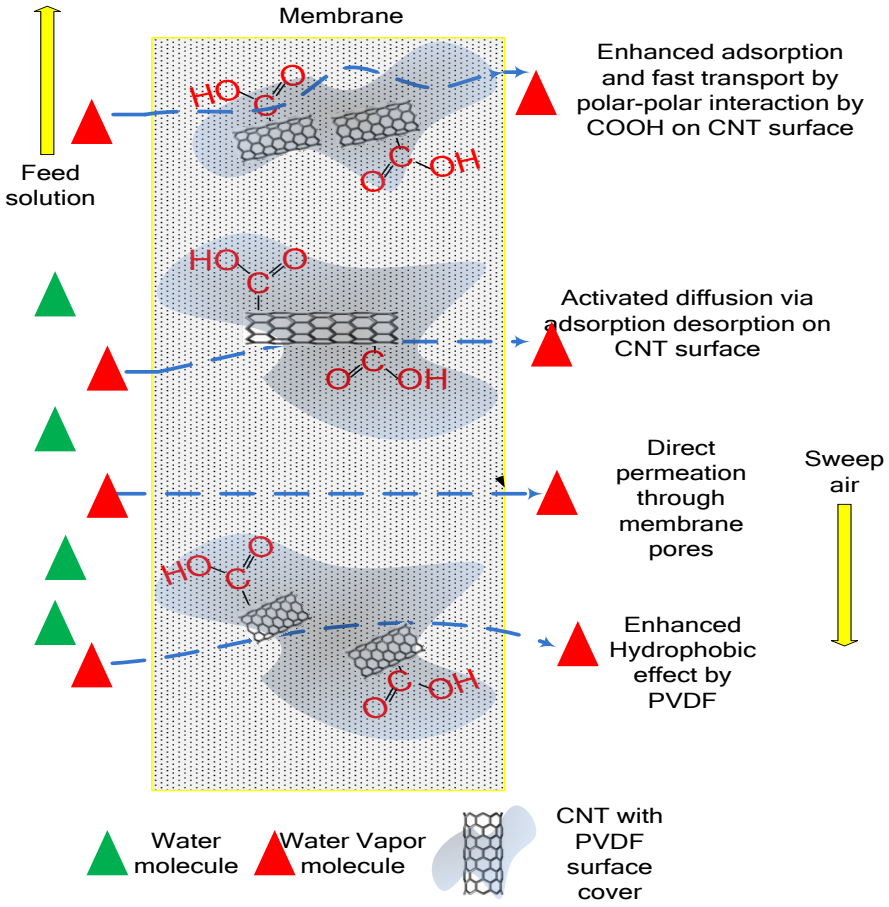

Figure 3.10 Mechanism of action on CNIM-f.

3.6 Conclusion

Carboxylated CNTs were incorporated into CNIM to enhance pure water flux in membrane distillation. With the incorporation of CNTs, the desalination performance was consistently higher than the conventional membrane. The carboxylated CNTs showed higher performance than their unfunctionalized analogs. The permeate flux achieved up to a maximum of 19.2 kg/m^2hr and salt reduction higher than 99.9% in all cases. These results indicate that the incorporation of carboxylated CNTs favorably altered the water-membrane interactions to enhance vapor permeability while preventing liquid penetration into the membrane pores. The membranes were stable over long periods of operation without any potential salt leakage.

CHAPTER 4

NANODIAMOND IMMOBILIZED MEMBRANE FOR ENHANCED DESALINATION VIA MEMBRANE DISTILLATION

4.1 Introduction

In the last two decades, detonation nanodiamonds (DNDs) which are typically produced by detonation method have attracted much attention. DNDs are carbon nanoparticles [63] with a truncated octahedral architecture that are typically about 2 to 8 nm in diameter. The DNDs have tetrahedral network structures and comprise of a diamond core (sp^3), a middle core (sp^{2+x}) and a graphitized outer core (sp^2) that is often partially oxidized [64]. They also have large grain boundary density, and low to negative electron affinity which has made them suitable for electronic applications [65]. They exhibit some interesting characteristics such as chemical stability, small size, inertness, large surface area, and high adsorption capacity [63]. Additionally, one of the distinct features of DNDs compared to carbon nanotubes and other carbon nanoparticles is the presence of a large number of different functional groups on the surface [66]. Consequently, they are being used in a variety of applications including coatings, polymer composites, lubricants, sensors, imaging, drug delivery, solar cells and electronics [67-76].

In previous Chapters 2 and 3, it has been demonstrated that by immobilizing carbon nanotube in different types of membranes alters the solute-membrane interactions, which is one of the major physicochemical factors affecting the permeability of a membrane. In line with this research, an important consideration is whether the DNDs could be introduced as a new class of nanomaterial for enhanced separation. The outer core of DNDs is somewhat similar to nanotubes and can serve as sorption sites that could

potentially be useful in enhancing permeation flux. For example, the immobilization of DND within conventional hydrophobic membrane for membrane distillation (MD) could lead to specific vapor-membrane interactions thereby enhancing water vapor permeation. This research aimed at initial immobilization of the DNDs within the hydrophobic membranes and the the modified membrane was investigated for sweep gas membrane distillation (SGMD) applications [77].

4.2 Experimental

The DND immobilized membrane (referred to as DNDIM) was prepared using Celgard type X30-240 (Celgard, LLC, and Charlotte, NC, USA) hollow fiber as the starting material and was constructed using the same procedure as mentioned in Chapter 2. The experimental set up and procedure for sweep gas membrane distillation was similar to that of Chapter 2.

4.3 Results and Discussion

The dispersion of DNDs in PVDF-Acetone solution after sonication, which was utilized for fabrication of DNDIM, is depicted in Figure 4.1. As shown, PVDF was chosen because the DNDs dispersed well in it. Scanning electron micrographs of the unmodified membrane, DNDIM and pristine DND crystals are shown in Figures 4.2 (a, b and c) respectively. As compared to the unmodified membrane (Figure 4.2 a), the incorporation of the DNDs in DNDIM is clearly evident in Figure 4.2b which depicts that the DNDs were uniformly distributed within the membrane. Thermal gravimetric analysis (TGA) was performed to determine the thermal stability of the DNDIM membrane. The TGA

curve is shown in Figure 4.3 and the amount of DND was found to be approximately 2% by weight. As observed, the thermal degradation of unmodified polypropylene membrane started at around 260^{o}C. The presence of DNDs increased the degradation temperature by 40^{o}C. This implies that the DNDs were highly stable and enhanced the thermal stability of the membrane. Incorporation of carbon nanotubes has shown similar behavior in terms of enhancing thermal stability [62]. This is an important factor for MD, where the elevated temperatures can be used for desalination. Additionally, the surface chemistries of the pristine DNDs were characterized by FTIR spectroscopy and from the spectra it was confirmed that surface functional groups such as hydroxyl, carboxylic, amines were present on the DNDs surface [78].

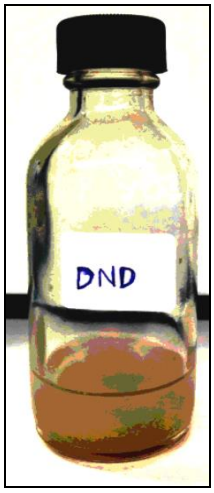

Figure 4.1 The dispersion of DNDs in PVDF-Acetone solution after sonication.

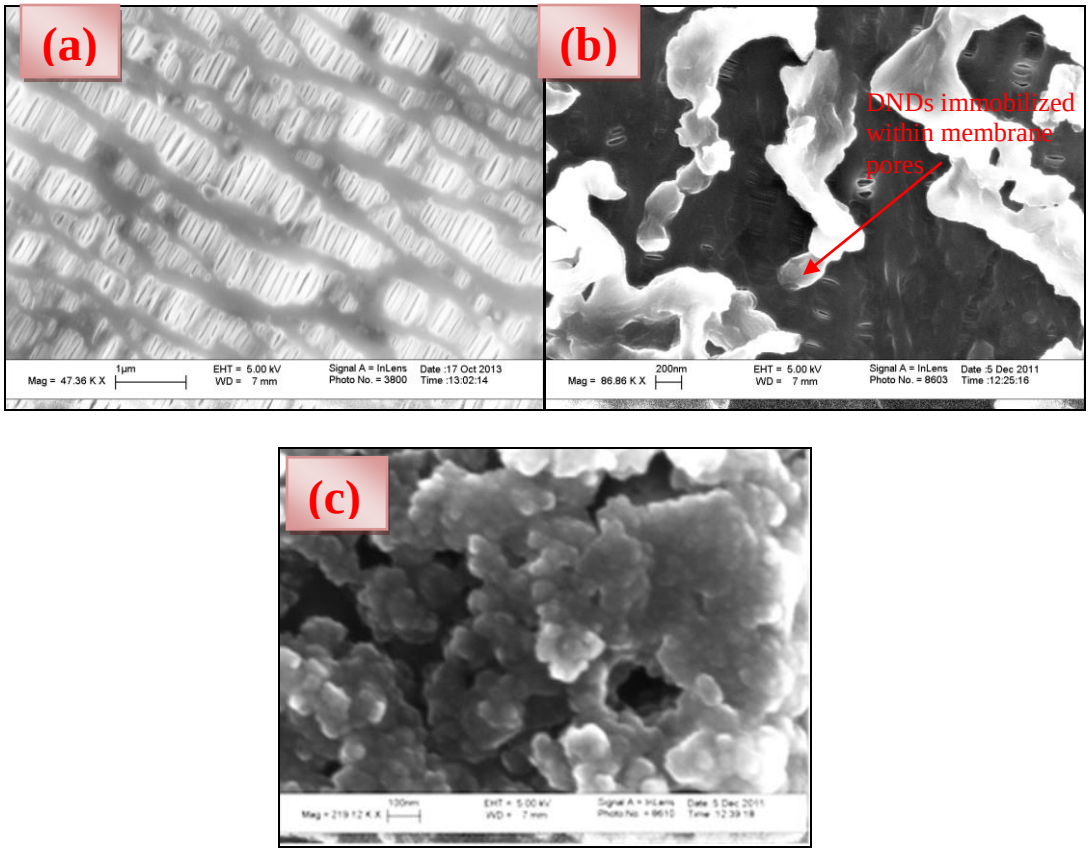

Figures 4.2 SEM images of (a) unmodified PP membrane (b) DNDIM (c) pristine DND crystals.

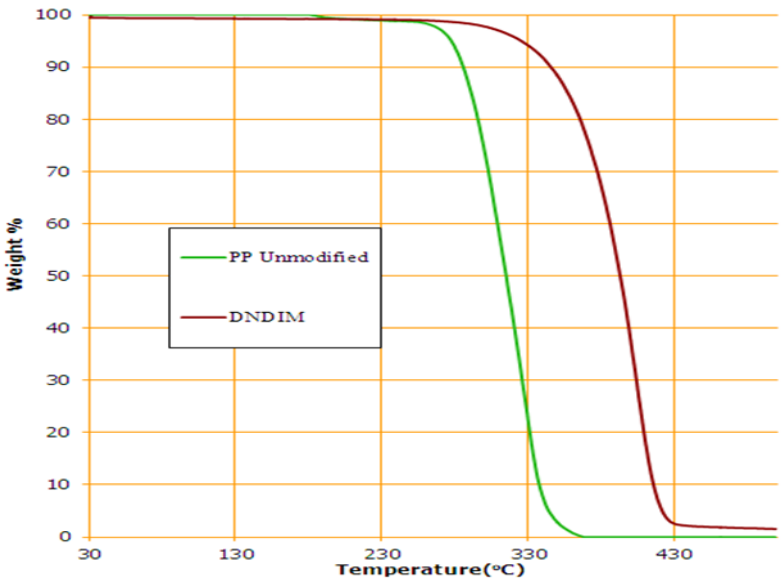

Figure 4.3 Thermo Gravitational Analysis of unmodified PP Membrane and DNDIM.

The DNDIM membranes were tested for MD. SGMD experiments were carried out in range of 70-90^{o}C at feed flow rate 10mL min^{-1}. As can be observed in Figure 4.4, increasing temperature increased permeate flux for both membrane types. This was due to the fact that the increased temperature difference created higher vapor pressure difference, thus enhancing overall water vapor flux. The DNDIM membrane showed enhanced flux at all temperatures. For example at 70^{o} C feed temperature, the flux using DNDIM was 10 lit/m^{2}h and was nearly the same (9.67 lit/m^{2}h) as that accomplished at 90^{o} C using the conventional unmodified membrane. At 90^{o}C, the flux using DNDIM reached as high as 13.8 lit/m^{2}h. The incorporation of DNDs generated significantly higher vapor flux at all temperatures. It is a well-established fact that DNDs have high thermal conductivity [63], which could potentially reduce the temperature gradient in the membranes, thus reducing flux. However, the low concentration of DND used here did not adversely affect temperature gradient or flux. These are in line with previous results published with carbon nanotubes [25].

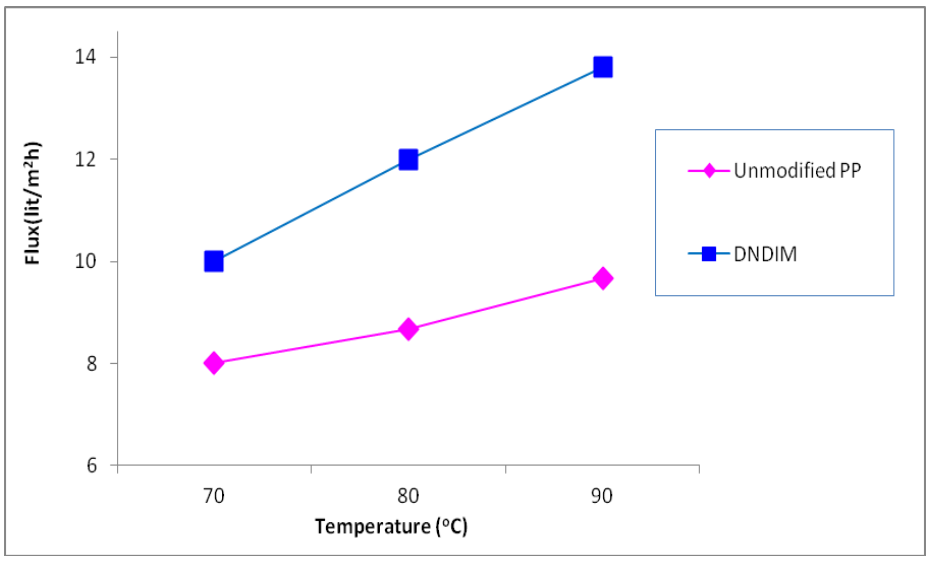

Figure 4.4 Effect of feed temperature on permeate flux at feed flow rate 10mL min^{-1} .

Desalination as a function of flow rate is shown in Figure 4.5. Experiments were carried out at a feed temperature 90^{o}C, in range of 7-24 mL min^{-1} feed flow rates. It was seen that for both membranes the increasing the flow rate first increased the permeate flux initially which then decreased. Both membranes showed similar trend, however, compared to unmodified membrane, DNDIM demonstrated higher flux at all feed flow rates. Enhancement as high as 83% was observed at an elevated flow rate of 24 mL min^{-1} for DNDIM compared to the unmodified membrane. DNDIM consistently showed higher resistance to the lowering of vapor flux.

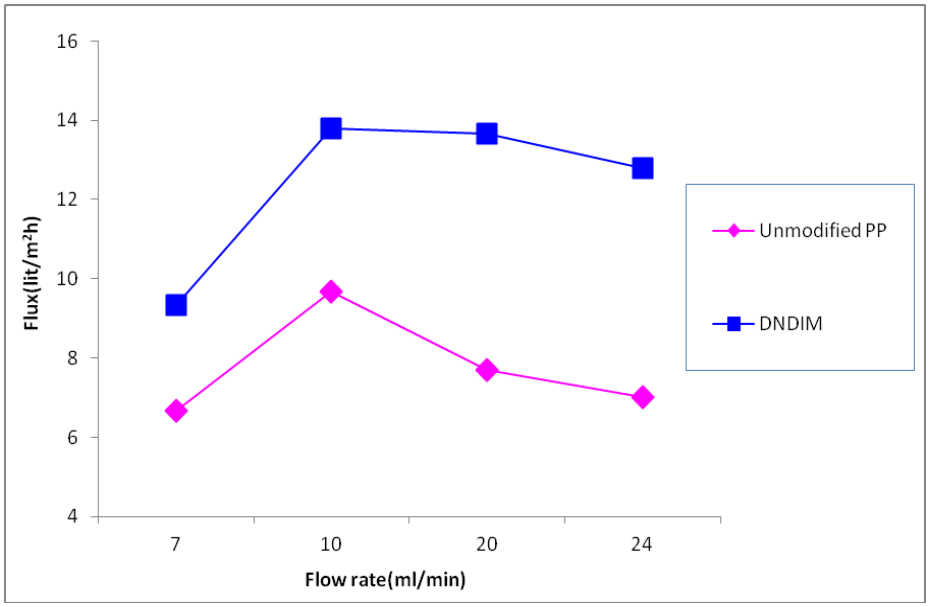

Figure 4.5 Effect of feed flow rate on permeate flux at feed temperature 90^{o}C.

Typically, water vapor flux in membrane processes tend to decrease with increase in salt concentration, this is primarily due to the decrease in water activity as concentration increases. Figure 4.6 depicts the effect of varying of feed concentration on permeate flux. The results showed a substantial decrease in flux for the unmodified

membrane from 9.67 lit/m^2h to 4 lit/m^2h. Typically, at an elevated feed concentration, a more significant boundary layer develops next to the membrane interface, which reduces driving force of mass transfer. This in turn leads to the decrease in permeate flux in case of unmodified membrane modules. On the other hand, DNDIM did not show significant lowering of flux. This was most likely due to the hydrophobic nature of the DNDs, which prevented the liquid phase penetration into the membrane pores. As observed from Figure 4.6, for DNDIM membrane, the flux was as high as 13.8 lit/m^2h and indicated that even at this extreme concentration, the DNDIM selectively allowed the passage of water vapor without any salt permeation.

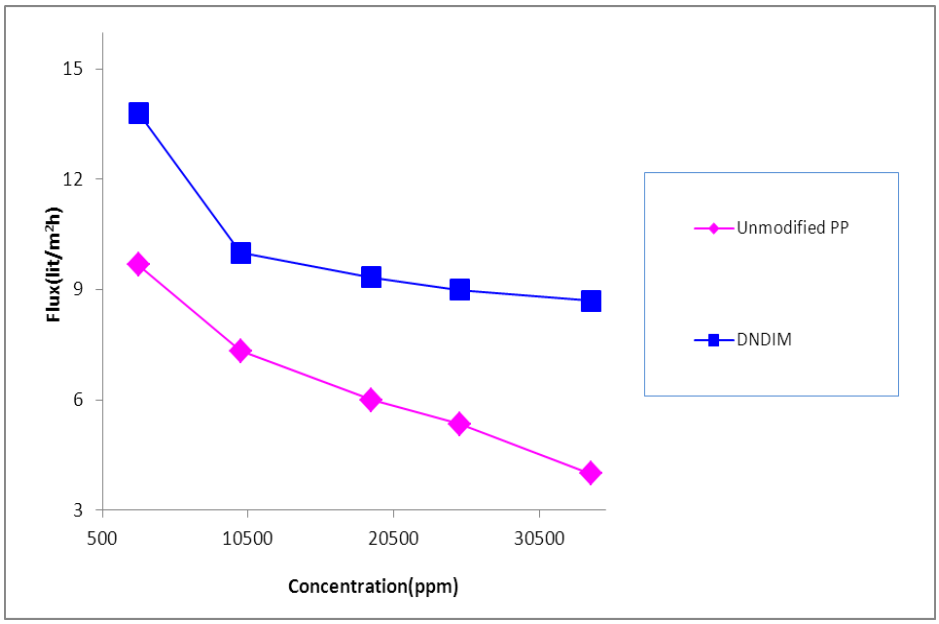

Figure 4.6 Effect of feed concentration on permeate flux at a feed flow rate of 10 mL min^{-1}, 90^oC.

Additionally, as observed from Table 4.1 and 4.2, the mass transfer coefficients (k) were found to be significantly higher for DNDIM as compared to the unmodified membrane. Table 4.1 indicates the effect of feed temperature on k. As observed, the

overall k was enhanced by presence of DNDs. For DNDIM, k varied from 8.9 $x10^{-08}$ to 5.5 $x10^{-08}$ at temperature ranging from 70-90^{o}C. A declining trend of (k) was found as the temperature increased. The temperature polarization becoming greater at higher temperature, a decrease of the membrane mass transfer coefficient was found when the temperature was increased. Furthermore, from Table 4.2 it was observed, that as the flow rate of feed water was increased from 7 to 24 mL min^{-1}, k in the unmodified membrane increased initially from $2.64x10^{-08}$ to $3.83x10^{-08}$ and then stayed more or less constant. Interestingly, for DNDIM the overall mass transfer enhancement was less affected at low flow rates but was higher at elevated flow rate. At a flow rate of 7 mL min^{-1}, the mass transfer coefficient of the DNDIM was 1.4 times higher than the unmodified membrane, but increased to 2 times at 24 mL min^{-1}. In general, the presence of the DNDs led to enhanced permeability of water vapor through the membrane, and the DNDIM showed a significantly higher overall mass transfer coefficient.

Table 4.1 Mass Transfer Coefficient at various feed temperatures at feed flow rate of 10 ml/min

	Mass transfer coefficient(kg/m^2.s.Pa)	
Temperature(^{o}C)	**Unmodified PP**	**DNDIM**
70	**7.13xE-08**	**8.92xE-08**
80	**5.09xE-08**	**7.04xE-08**
90	**3.83xE-08**	**5.47xE-08**

Table 4.2 Mass Transfer Coefficient at Various Feed Flow Rates at Feed Temperature 90^{o}C

	Mass transfer coefficient(kg/m^2.s.Pa)	
Feed flow rate(ml/min)	**Unmodified PP**	**DNDIM**
7	**2.64xE-08**	**3.70xE-08**
10	**3.83xE-08**	**5.47xE-08**
20	**3.05xE-08**	**5.42xE-08**
24	**2.77xE-08**	**5.07xE-08**

4.4 Proposed Mechanism

The proposed mechanisms of enhanced water vapor transport in the presence of DNDs are shown in Figure 4.7, where DNDs serve as selective sorption sites for water vapors. Since the outer core of the DNDs is graphitic and quite hydrophobic, they decrease pore wetting while enhancing the transport of pure water vapor. This was confirmed by contact angle measurements where unmodified PP had a contact angle of 110^{o} and DNDIM of 119^{o}, which showed that the hydrophobicity of the DNDIM was higher due to inclusion of DNDs which favored the repulsion of the liquid water. Additionally, the DNDs possess a graphitic ring structure with additional -COOH and -OH groups on its surface which leads to specific interactions with the water vapor molecules leading to enhanced flux. It is also well established that the DNDs have higher surface area, which may lead to enhanced adsorption, which further leads to enhanced flux. The higher thermal conductivity of the DNDs has the potential to reduce the temperature gradient in

the membranes, however the amount of DNDs is so small and they are sparsely distributed throughout the matrix and we believe that they do not reduce the temperature gradient.

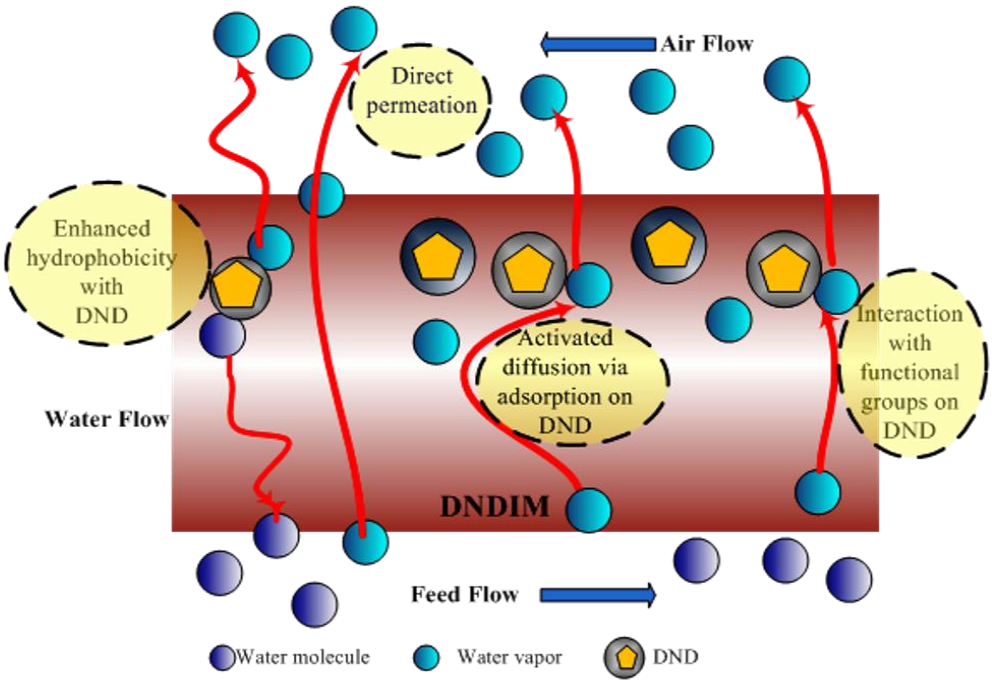

Figure 4.7 Proposed Mechanism for DNDIM.

4.5 Conclusion

DNDs were effective as a new generation of nanomaterials for modifying conventional hydrophobic membranes to enhance water vapor flux in membrane distillation. Results show that the DNDs were well imbedded within the membrane. The desalination performance was consistently higher using the DNDIM than the unmodified membrane. Permeate flux achieved up to a maximum of 13.8 lit /m^2h and salt reduction of 99.9%. These results indicate that the incorporation of DNDs favorably altered the water-membrane interactions to enhance vapor permeability while preventing liquid penetration into the membrane pores.

CHAPTER 5

FLUX ENHANCEMENT IN DIRECT CONTACT MEMBRANE DISTILLATION BY IMPLEMENTING CARBON NANOTUBE IMMOBILIZED MEMBRANE

5.1 Introduction

The objective of this chapter is to investigate the inclusion of functionalized carboxylated carbon nanotube on a hydrophobic polytetrafluoroethylene (PTFE) membrane for direct contact membrane distillation desalination application. As mentioned in previous chapters, Membrane Distillation (MD) has emerged as an alternative to conventional desalination techniques such as reverse osmosis and thermal distillation. Though Sweep Gas Membrane Distillation technique has been utilized for desalination applications, Direct Contact Membrane Distillation (DCMD) is the most commonly used configuration in which a porous hydrophobic membrane is imposed between the aqueous brine solution at a higher temperature and a colder distillate on the permeate side [79-80]. In DCMD, water vapor diffuses through a porous membrane and condenses into the cold distillate. The main effort in optimal design of such DCMD membrane involves the maximization of solute rejection and flux, with high feed side heat transfer coefficient [81-82] but low thermal conduction by the membrane. A key component in such a process is the membrane itself because it determines both water vapor flux and selectivity. Previously, it was demonstrated that by immobilizing CNTs within the membrane pores, the solute-membrane interactions could be altered, which is one of the major physicochemical factors affecting the permeability and selectivity of a membrane for MD application. CNTs in such carbon nanotube immobilized membrane (CNIM) provide additional pathways for water vapor transport. So far, these membranes have been used in sweep gas membrane distillation applications and have demonstrated superior performance.

However, an important consideration that is yet to be fully exploited is whether carboxylated CNTs could further lead to specific interactions with water vapour and if such membranes could be further employed in DCMD configuration. Of particular interest is the immobilization of the CNTs on a hydrophobic polytetrafluoroethylene membrane backbone.

5.2 Experimental

The membrane module used for DCMD set up was a flat, disk-shaped module, with a gasket diameter of 4.3cm and an effective membrane area of 14.5 cm^2. The membrane used was that of polytetrafluroethylene (PTFE) laminated onto a non woven Polypropylene fabric support for improved strength and temperature handling (Gore-Tex). The feed used in these experiments ranged from 3000-34000 ppm NaCl solutions (Sigma Aldrich) and permeate used was that of deionized water. Both hot and cold sides were circulated through the module using a peristaltic pump (Cole Parmer, model 7518-60). The preheated hot feed solution traveled through a heat exchanger, which was used to maintain the desired temperature through out the experiment and was fed to one side of the DCMD cell module. The hot feed was recycled to the feed tank and permeate was obtained in the distillate tank. Inlet and outlet temperatures of the feed and distillate were monitored continuously throughout the experiment. Viton and different PFA tubings and connectors (Cole Parmer) were used to make connections in the experimental set up. The ionic strength of the original feed solution and permeate were measured using a Jenway Electrode Conductivity Meter 4310. The schematic of DCMD experimental system is shown in Figure 5.1 and the laboratory scale DCMD set up is shown in Figure 5.2. Each

experiment under any given parameter was run for 2 hours. Each experiment was repeated thrice for reproducibility.

For the synthesis of MWCNT-COOH, pristine MWCNT was purchased from Cheap Tubes, Inc., Brattleboro, VT, USA. The functionalized CNT membrane (referred to as CNIM-f) was prepared using PTFE membrane with a non woven fabric support and a pore size of 0.4 um. For the preparation of CNIM-f, each of 10 mg of MWCNT-COOH were dispersed in a solution containing 0.2 mg of Poly tetrafluroethylene (PTFE) powder of 1um particle size (Sigma Aldrich) in 10 ml of Fluorinert FC-40 solvent (Sigma Aldirch) by sonicating for three hours. The PTFE-nanotube dispersion was then utilized for membrane fabrication.

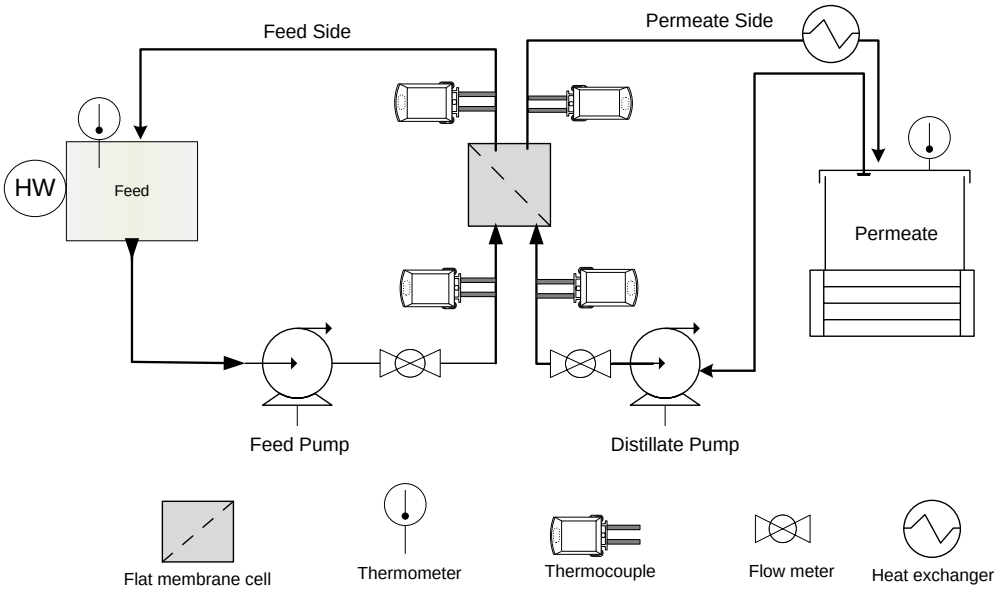

Figure 5.1 Schematic diagram of experimental set up of direct contact membrane distillation.

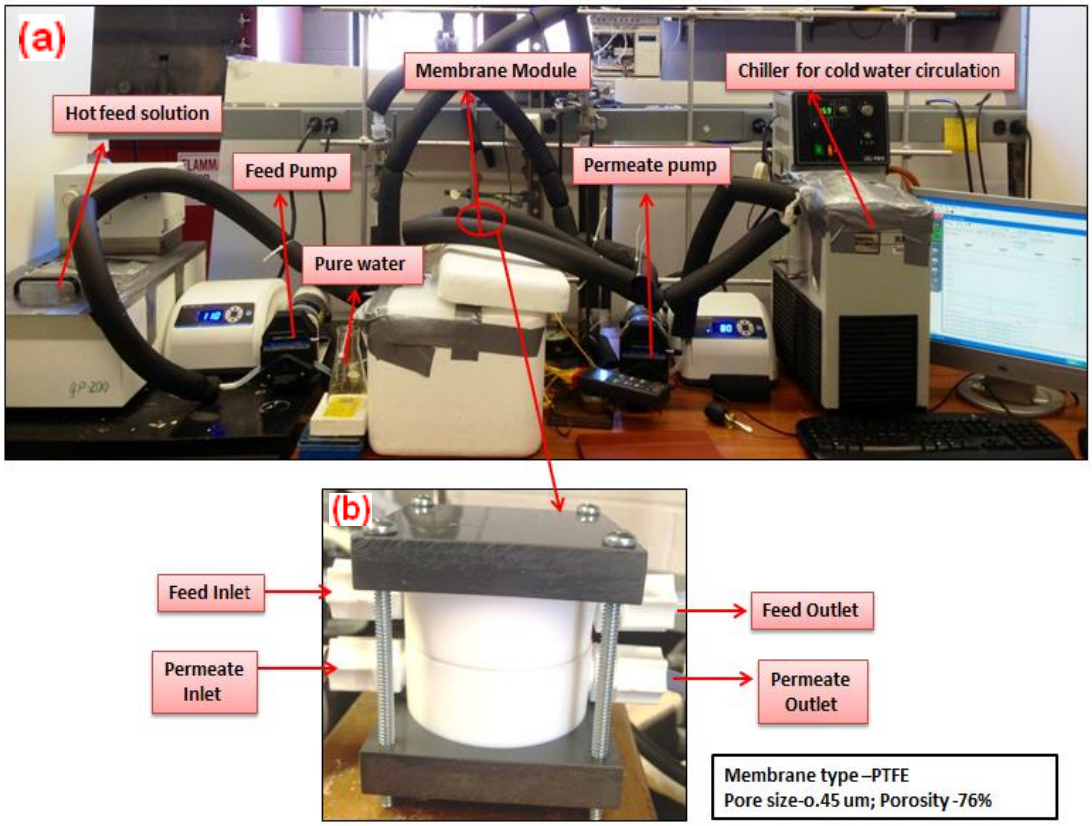

Figure 5.2 a) Laboratory set up b) Flat cell membrane module.

5.3 Membrane Characterization

The morphology of CNIM-f was studied using a scanning electron microscopy (SEM, Model LEO 1530, (Carl Zeiss SMT AG Company, Oberkochen, Germany). This was done by cutting the membranes into 0.5 cm long pieces and coating with carbon films. Confocal Raman imaging and Raman spectra were measured using a Thermo electron Nicolet Raman spectrometer. Furthermore, thermal gravitational analysis (TGA) was performed using a Perkin Elmer Pyris 7 TGA instrument with a heating rate of 10^{o}C/min under air atmosphere to study the thermal stability of the membrane. To verify the hydrophobic-hydrophilic nature of the unmodified PTFE and CNIM-f, water droplets (2

µl) were deposited using a micro syringe Hamilton (0-100 µl) on the PTFE and the CNIM-f. The particle positions were recorded and the contact angle was measured using a digital video camera mounted at the top of the stage. Five readings were obtained and the average value together with the standard deviation is reported in this study.

Gas permeation tests were performed to measure the effective surface porosity over the effective pore length of the porous membrane. The measurements were made according a method published before [83]. The total molar gas permeation flux per unit trans membrane pressure difference across the porous membrane ($J_i/\Delta p$) is described by Equation. (1) where the first term represents the contribution from Knudsen flow and the second term is due to Poiseuille flow:

$$\frac{J_i}{\Delta p} = \frac{2}{3}\left(\frac{8RT}{\pi M}\right)^{0.5} \frac{1}{RT}\frac{r\varepsilon}{L_p} + \frac{\bar{p}}{8\mu RT}\frac{r^2\varepsilon}{L_p} \qquad (5.1)$$

Here ε is surface porosity, r is mean pore radius of the membrane, is gas viscosity, R is gas constant, $\bar{p}$ is the mean pressure (average of feed and permeate side pressure), M is molecular weight of gas, L_p is effective pore length and T is temperature (K). The gas permeation flux per unit driving force ($J_i/\Delta p$) is calculated as follows:

$$\frac{J_i}{\Delta P} = \frac{N_{t,i}}{A_t} \tag{5.2}$$

Here $N_{t,i}$ is total molar gas permeation rate (mol s^{-1}), $\bar{p}$ is the trans membrane pressure difference across the membrane area A_t. The total gas permeation rate through the membrane at different pressures was measured employing a soap bubble flow meter for low flow rates of nitrogen. From a plot of the nitrogen flux as ($J_i/\Delta p$) against the mean gas pressure $\bar{p}$, the mean pore size (r) and the effective surface porosity over pore length, ε/L_p, can be obtained from the slope S_o and the intercept I_o as follows:

$$r = \frac{16}{3}\left(\frac{S_o}{I_o}\right)\left(\frac{8RT}{\pi M}\right)^{0.5}\mu_i \tag{5.3}$$

$$\frac{\varepsilon}{L_p} = \frac{8\mu_i RTS_o}{r^2} \tag{5.4}$$

5.4 Results and Discussions

Scanning electron micrographs of the original PTFE membrane and CNIM-f are shown in Figures 5.3 a, b and c. Figure 5.3 a, b illustrates the top and bottom surface of the unmodified PTFE membrane. The top surface clearly depicts the membrane pores and the

bottom surface depicts the non woven laminated support. The change in morphology in Figure 5.3 c clearly indicates the incorporation of the carboxylated CNTs within the pores. The presence of CNT-COOHs as slender strands within the membrane pores were absent in unmodified PTFE membrane. Raman spectra of the unmodified PTFE membrane and CNIM-f are depicted in Figure 5.3d. Dominant raman bands of 291, 386, 774, 1329, 1362 cm^{-1} of PTFE backbone as observed in both spectra could be attributed to CF_2 wagging, CF_2 twisting, CF_2 symmetric stretch, CF_2 asymmetric stretch and CF stretching, respectively [84]. A careful observation in case of CNIM-f spectra revealed an up shift of Raman bands to 1581 and 1600cm^{-1}. This could be attributed to the carboxylic group in the D-band region of CNTs (3.7 cm^{-1}) and G-band region (4.6 cm^{-1}) at 1597–1603 cm^{-1}, respectively. This shift of the Raman response of the oxidized sample could be caused by doping effects (electron doping) upon acid treatment. In addition, Figure 5.3e depicts Raman microscopic image of CNIM-f. The dark patches of CNT-COOHs are distinctly visible in CNIM-f.

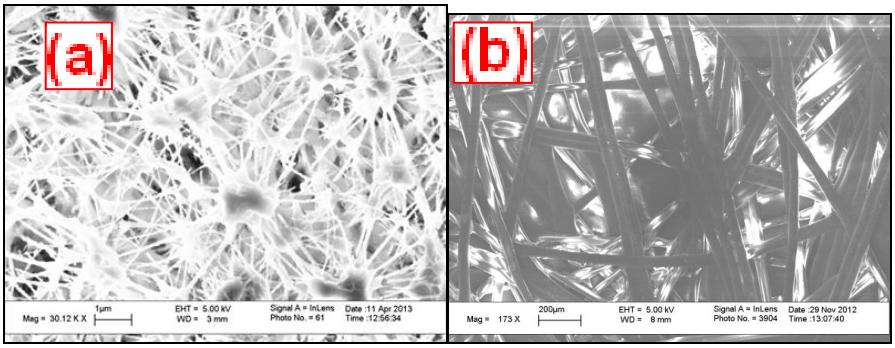

Figure 5.3 Scanning Electron Micrographs (a) PTFE unmodified active layer; (b) support Layer; (c) CNIM-f (d) Raman analysis spectra of unmodifed PTFE and CNIM-f (e) Raman image of CNIM-f .

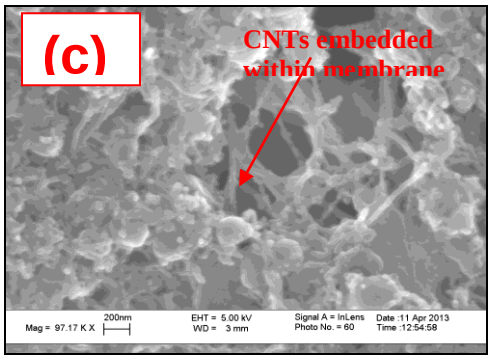

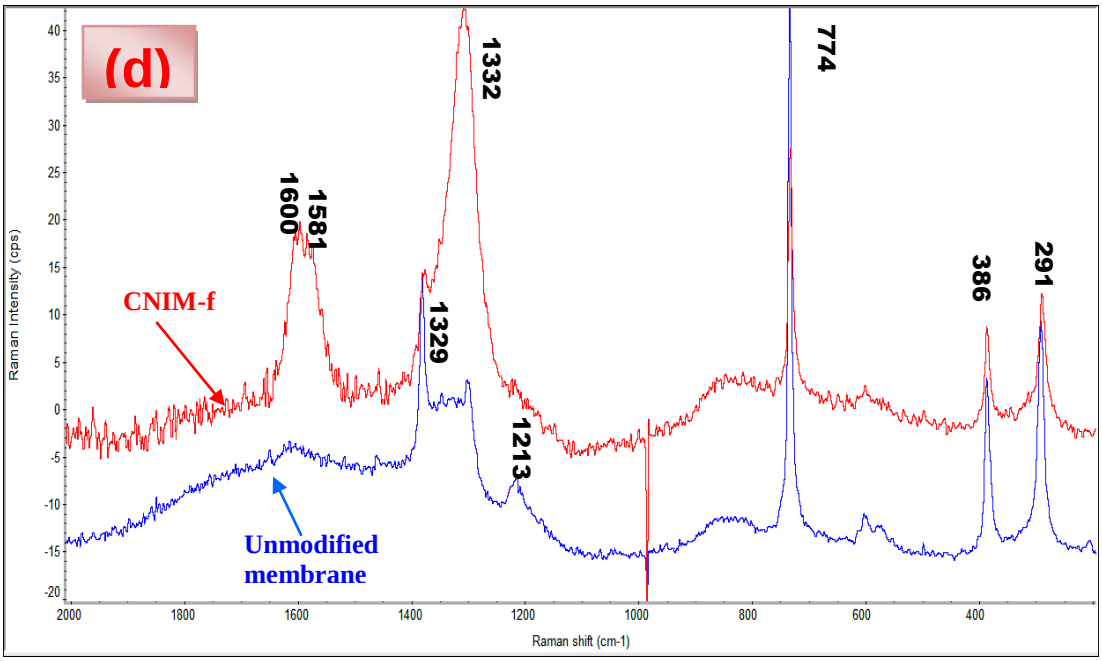

Figure 5.3 Scanning Electron Micrographs (a) PTFE unmodified active layer; (b) support Layer; (c) CNIM-f (d) Raman Analysis spectra of unmodifed PTFE and CNIM-f (e) Raman image of CNIM-f (cont).

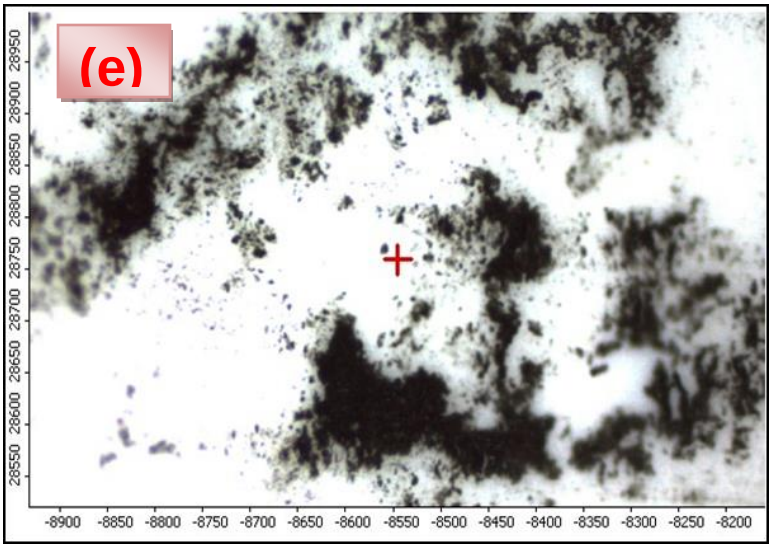

Figure 5.3 Scanning Electron Micrographs (a) PTFE unmodified active layer; (b) support Layer; (c) CNIM-f (d) Raman analysis spectra of unmodifed PTFE and CNIM-f (e) Raman image of CNIM-f (cont).

The TGA thermogram as depicted in Figure 5.4 shows that the CNIM-f membrane showed its first weight loss at 218^{o}C due to the onset of thermal degradation of unmodified PTFE membrane followed by final decomposition at 460^{o}C, which may be due to the inclusion of CNT-COOHs in the PTFE polymer layer. This implies that the CNIM-f was highly stable and inclusion of the hydrophobic polymer enhanced the overall thermal stability of the membrane.

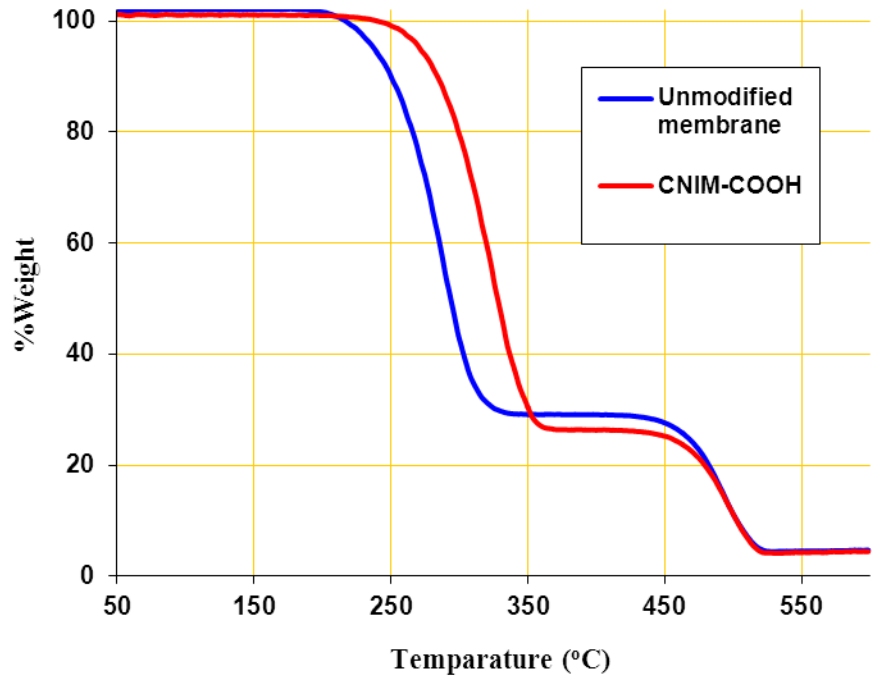

Figure 5.4 Thermal Gravimetric Analysis of Unmodified Membrane and CNIM-f.

The change in hydrophobicity of the unmodified PTFE and CNIM-f is shown in Figure 5.5a and Figure 5.5b respectively. The photograph of the water drop on unmodified PTFE membrane exhibited a contact angle of 100^{o} indicating the hydrophobic nature (Figure 5.5a). On the other hand, after immobilization with MWCNT-COOH for CNIM-f membrane, the contact angle was 106^{o}, as observed from Figure 5.5b.

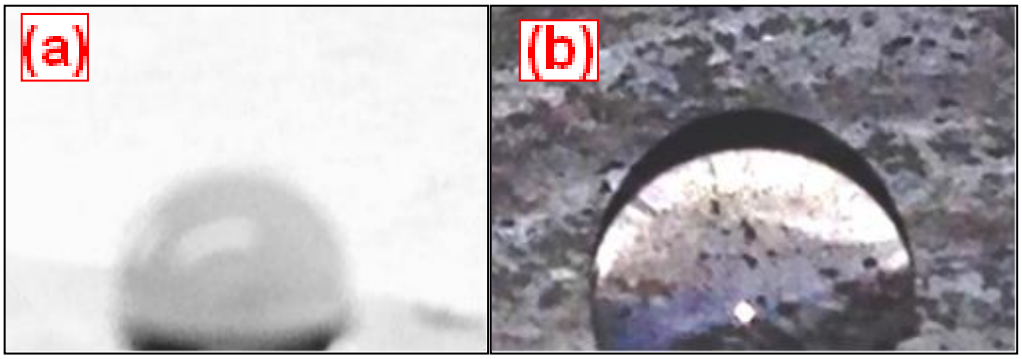

Figure 5.5 Photograph of water drop on (a) unmodified PTFE membrane (b) Photograph of water drop on CNIM-f .

Nitrogen gas permeation flux through the flat sheet membrane was measured at different pressures and plotted as ($J_i/\Delta p$) against the mean pressure $\bar{p}$. The porosity was determined by mass difference. The weights of the membrane with its support and the support layer without the active layer were measured by a BP221-S balance. The thickness of each membrane cross section was measured three times with a Mitutoyo IP65 meter. Each measurement was done three times from different sections of the membrane and an average was reported as membrane thickness. The porosity of membrane active layer was calculated as follows:

$$\varepsilon = 1 - \frac{(m_{total} - m_{\sup port}) / \rho}{V} \qquad (5.5)$$

where ρ is the material density of the active layer, in which a midpoint in density range of the polymer density was used (an error less than 3%); m_{total} and $m_{support}$ are, respectively

the masses of the membrane with the support layer and the support layer only; V is the volume of active layer, which was calculated by multiplying the area with the active layer thickness. The nominal pore size of the flat sheet membrane was found to be 0.03 micron, porosity of 72% and the effective porosity over pore length (ε/L_p) was found to be 3.09 x 10^6. As anticipated, the effective porosity over pore length did not show any significant change in the CNIM because only a small amount of CNT inclusion was made on the surface of the membrane.

The effect of feed temperature on membrane flux of the CNIM and the unmodified PTFE membrane is shown in Figure 5.6, where feed and permeate flow rates were fixed at 212 ml min^{-1} and 164 ml min^{-1} , respectively. The permeate fluxes of both membranes increased with feed temperature. This was due ot the fact that the increased temperature difference created higher vapor pressure difference, thus enhancing water vapor flux . Permeate flux reached their maximum at 80^o C with maximum flux for CNIM reaching a maximum of 77 kg/m^2h. Overall, CNIM-f showed consistently higher flux at all temperatures, although the effects seemed to be most pronounced at lower feed temperatures of 60-65 ^oC. At a feed temperature of 60^oC the CNIM showed a flux of 60 kg/m^2h, which was nearly the same accomplished by using unmodified PTFE membrane at around 70^o C. Therefore CNIM demonstrated significantly higher eco-efficiency, because operations could be carried out at significantly lower temperature thereby making it an overall greener process.

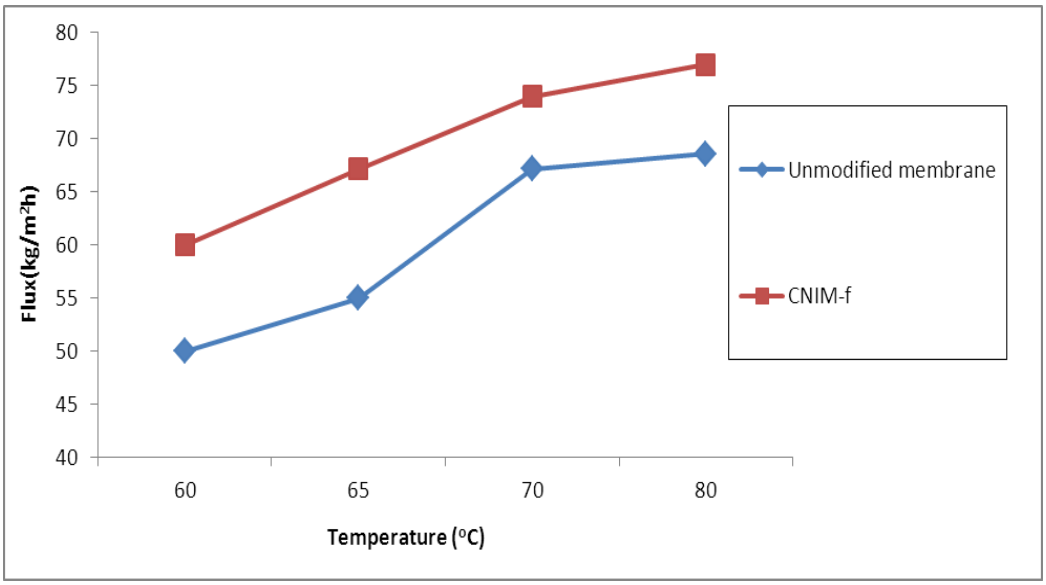

Figure 5.6 Effect of feed temperature on permeate flux at feed flow rate of 212 ml min^{-1} , permeate flow rate 164 ml min^{-1} .

Effect of feed flow rate on permeate flux is illustrated in Figure 5.7. The feed flow rate was varied from 30 to 212 ml min^{-1} while the permeate side flow rate was fixed at 164 ml min^{-1} and the permeate side temperature was maintained at 20^{o}C. Permeate flux increased as the feed velocity increased for both unmodified PTFE membrane and CNIM. At a feed flow rate of 36 ml min^{-1}, both membranes showed almost identical flux. This could be attributed to the fact that, at a low flow rate the residence time was long and the by the boundary layer effects were predominant and the CNTs did not seem to be that significant in flux enhancement. At a high flow rate when turbulence reduced the temperature polarization and boundary layer effects, flux was controlled by the properties of active layer of CNIM, flux enhancement was significant and reached as high as 73 kg/m^2h at a flow rate of 212 ml min^{-1}. This represented an overall 26% enhancement in flux.

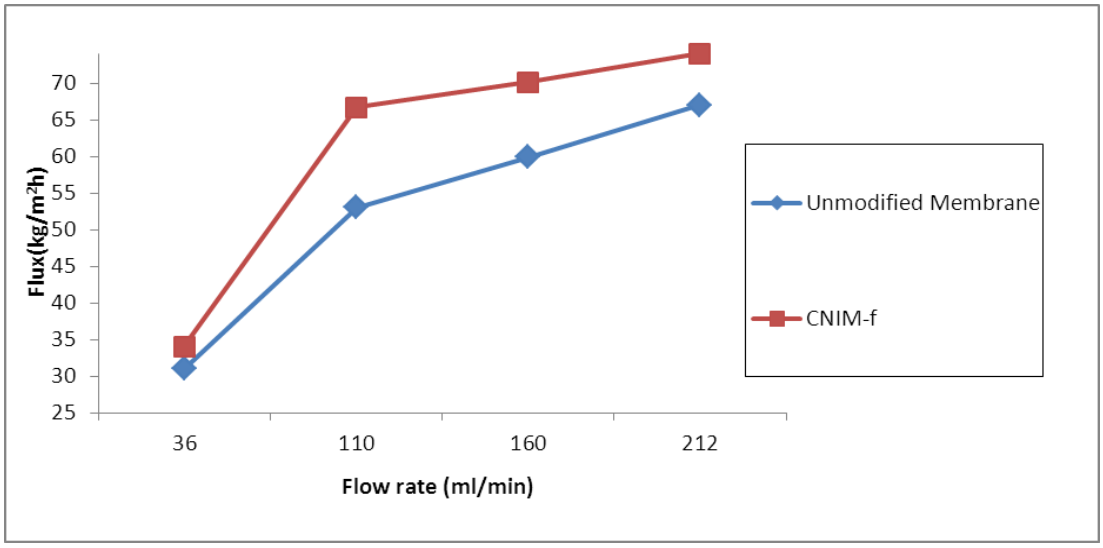

Figure 5.7 Effect of feed flow rate on permeate flux at feed temperature of 70°C, permeate flow rate 164 ml min^{-1}.

Figure 5.8 shows the effect of varying feed concentration on permeate flux. As mentioned in previous Chapters 3 and 4, concentration polarization is more important at higher feed concentrations, where a thicker boundary layer reduces driving force of mass transfer. Consequently, this leads to the decrease in permeate flux. In the case of unmodified PTFE membrane the decrease in flux was quite significant dropping from 60 kg/m^2h to 44 kg/m^2h as the concentration increased from 4000 ppm to 34,000 ppm. On the other hand, the decrease in permeate flux in CNIM was not as significant for CNIM, where the drop for the same concentration range was from 75 kg/m^2h to 69 kg/m^2h. Therefore CNIM represented some excellent advantages at 34,000 ppm, and represented an enhancement of 54%. This is attributed to the fact that the presence of CNTs increased the surface roughness that prevented the formation of stable boundary layers. This could be confirmed in Figure 4c.

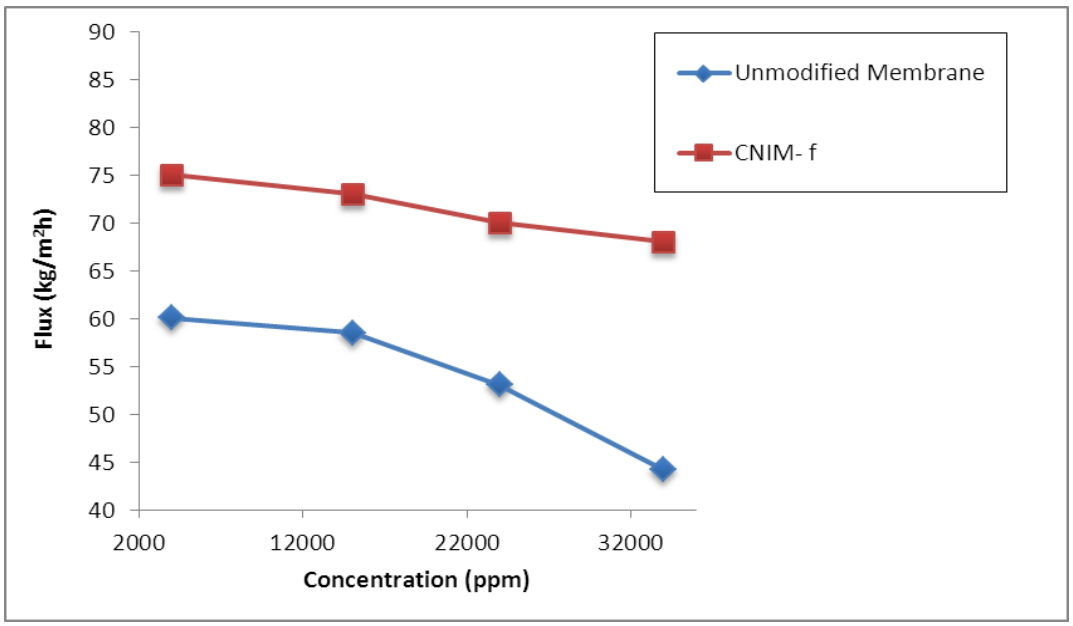

Figure 5.8 Effect of feed concentration on permeate flux at feed temperature 70^{o}C and feed flow rate 212 ml min^{-1}, permeate flow rate 164 ml min^{-1}.

As could be observed from Figure 5.9, mass transfer coefficient increased linearly with increasing feed temperature for both membranes. CNIM showed higher mass transfer coefficients than the unmodified membrane at all feed temperatures. Table 5.1 shows that mass transfer coefficients increased with feed flow rate and the values were significantly higher for CNIM with the enhancement in mass transfer coefficient was higher at a low flow rate reaching up to 40%.

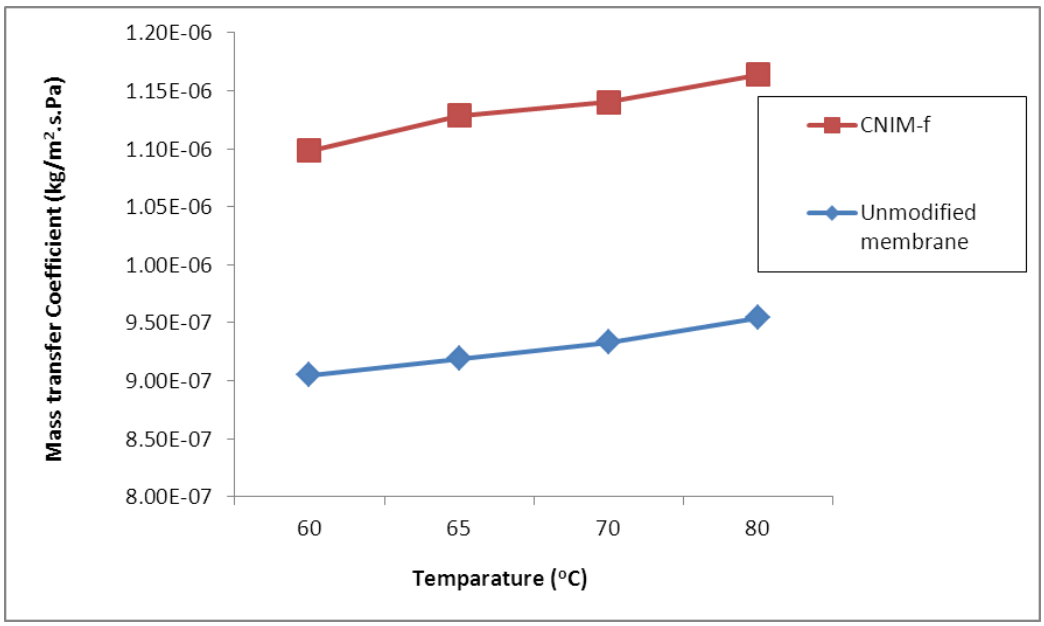

Figure 5.9 Variation of Mass transfer coefficient at various feed temperature at feed flow rate of 212 ml min^{-1}, permeate flow rate 164 ml min^{-1}.

Table 5.1 Mass Transfer Coefficient at Various Feed Flow Rate at Feed Temperature 70^{o} C

	Mass transfer coefficient (kg/m^2.s.Pa)	
Flow rate (ml/min)	**PTFE**	**CNIM-f**
36	**4.3E-07**	**5.2E-07**
110	**7.4E-07**	**1.0E-06**
160	**8.3E-07**	**1.1E-06**
212	**9.3E-07**	**1.1E-06**

The permeation flux obtained by our current DCMD configuration was appreciably higher compared to the result obtained by our previous report by sweep gas membrane distillation where a sweep gas was used to capture the permeated water vapor [62]. In current DCMD configuration, though the enhancement in flux and mass transfer

coefficient for CNIM-f membrane over unmdofied PTFE at a feed temperature of 80^{o} C at 34,000 ppm concentration was 54% and 24% respectively as compared to the flux and mass transfer enhancement of 95% respectively for SGMD configuration. It is worth mentioning that the overall flux achieved by the DCMD configuration was significantly higher than that achieved by CNIM SGMD [62]. This is in line with what has been reported before [85]. The higher flux has been attributed to the higher capacity of the cold liquid stream for absorption and condensation of the permeated vapor than an air stream as in SGMD [86].

5.5 Proposed Mechanism

A significantly higher flux was observed for CNIM as compared to the unmodified PTFE membrane. This was attributed to the fact that the CNTs served as sorbent sites for vapor transport while rejecting the liquid water. The carboxylated CNTs are more polar and they provided higher sorption for the water vapors, thus enhancing flux. Although the hydrophilic CNT-COOH could be expected to decrease the overall hydrophobicity of the membrane and also interact with the sodium ions, our dispersion of carboxylated CNTs consisted of a hydrophobic encapsulation (Figure 5.10), which prevented water as well as Na^{+} ions from reaching the CNTs.

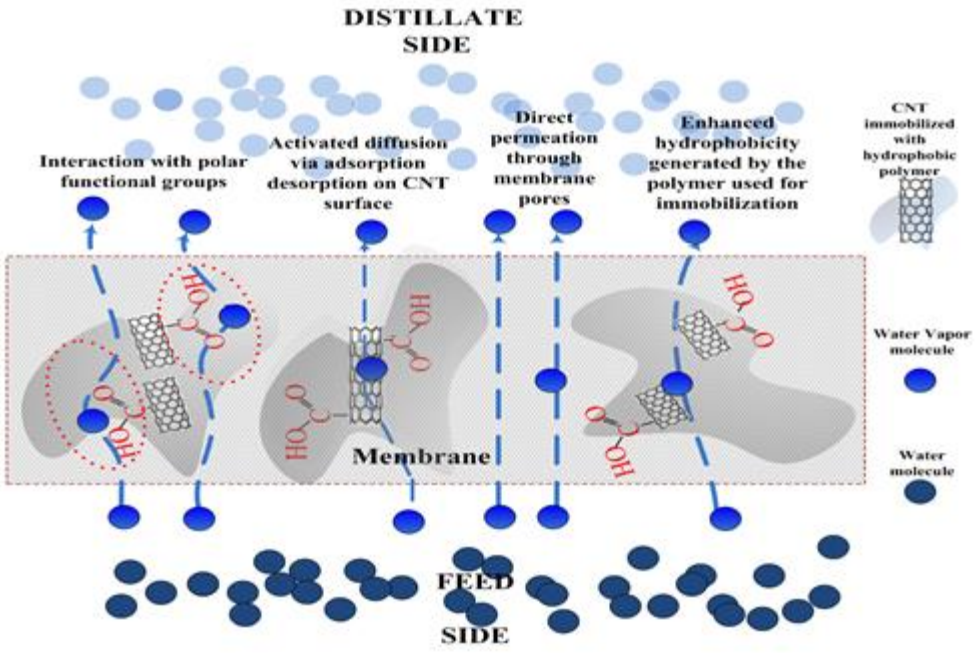

Figure 5.10 Mechanism of action on CNIM-f.

5.6 Conclusion

Carboxylated CNTs/PTFE dispersion was incorporated within PTFE membrane to enhance pure water flux in direct contact membrane distillation mode. The desalination performance was consistently superior using the CNIM-f as compared to the unmodified PTFE membrane. The permeate flux achieved up to a maximum of 77 kg/m^{2}hr and salt reduction higher than 99.9% . Mass transfer coefficients were calculated to evaluate the mass transfer efficiency of the process and CNIM-f had mass transfer coefficients higher than that of unmodified PTFE membrane under all operational conditions. CNIM-f also showed stability over longer period of time without any fouling and wetting issues. These results suggest that the incorporation of carboxylated CNTs - PTFE dispersion to prevent direct interaction with water, favorably altered the water-membrane interactions to enhance vapor permeability while preventing liquid penetration into the membrane pores.

CHAPTER 6

FABRICATION AND CHARACTERIZATION OF NOVEL HYDROPHOBIC FUNCTIONALIZED CARBON NANOTUBE MEMBRANE FOR DIRECT CONTACT MEMBRANE DISTILLATION DESALINATION

6.1 Introduction

The objective of this work was to determine if hydrophobic functionalized carbon nanotube immobilization on the PTFE membrane backbone could further enhance the vapor flux as compared to hydrophilic functionalized carbon nanotube for desalination via direct contact membrane distillation.

6.2 Experimental

The membrane module used for DCMD set up was similar to those used in Chapter 5. The experimental set up for the DCMD configuration was similar to that of Chapter 5. A new functionalized CNT membranes were fabricated, namely CNIM-ODA. The ODA (Octadecylamine) functionalized CNT membrane (referred to as PTFE-ODA) was prepared using PTFE composite membrane with a non woven fabric support and a pore size of 0.4um. For the preparation of CNIM-ODA, each of 0.01gm of MWCNT-ODA were dispersed in a solution containing 0.005gm of Poly tetrafluroethylene (PTFE) powder of 1µm particle size (Sigma Aldrich) in 10 ml of Fluorinert FC-40 solvent (Sigma Aldirch) by sonicating for three hours. This PTFE-ODA dispersion was then utilized for membrane fabrication on the feed side of the membrane. The morphology of CNIM-f was studied using a scanning electron microscopy (SEM, Model LEO 1530, (Carl Zeiss SMT AG Company, Oberkochen, Germany). This was done by cutting the membranes into 0.5 cm long pieces and coating with carbon films. Confocal Raman

imaging and Raman spectra were measured using a Thermo electron Nicolet Raman spectrometer. Furthermore, thermal gravitational analysis (TGA) was performed using a Perkin Elmer Pyris 7 TGA instrument to study the thermal stability of the membrane.

6.3 Results and Discussion

Scanning electron micrographs of the unmodified PTFE membrane and the bilayer functionalized membranes are depicted in Figures 6.1. Figure 6.1a illustrates the top and surface of the unmodified membrane. The top surface clearly depicts the membrane pores. The change in morphology in Figure 6.1b clearly indicates the incorporation of the octadecylamine CNTs of the top membrane surface. As revealed from figure 6.1b, the MWCNT-ODA was well immobilized within the membrane surface of the PTFE membrane.

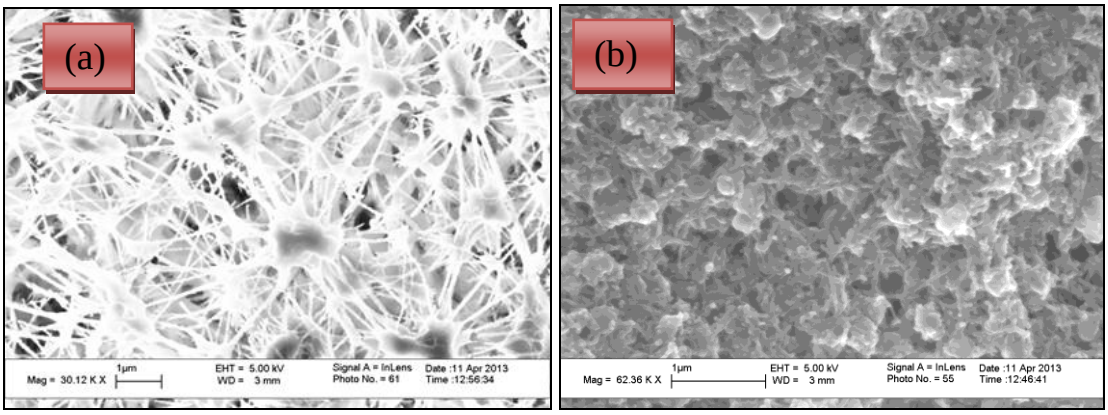

Figure 6.1 Scanning Electron Micrographs (a) PTFE unmodified active layer (b) CNIM-ODA .

Figure 6.2a depicts the Raman imagery of top hydrophobic functionalized membrane surface. Dominant raman bands of 291, 386, 774, 1329, 1362 cm^{-1} of PTFE backbone as observed in both spectra could be attributed to CF2 wagging, CF2 twisting, CF2

symmetric stretch, CF2 asymmetric stretch and CF stretching, respectively. A careful observation in case of CNIM-ODA spectra revealed a peak at 1586 cm^{-1} and 2611 cm^{-1} which could be attributed to the amine group and the secondary amine connected to the octadecyl amine chain of the MWCNT-ODA, respectively.

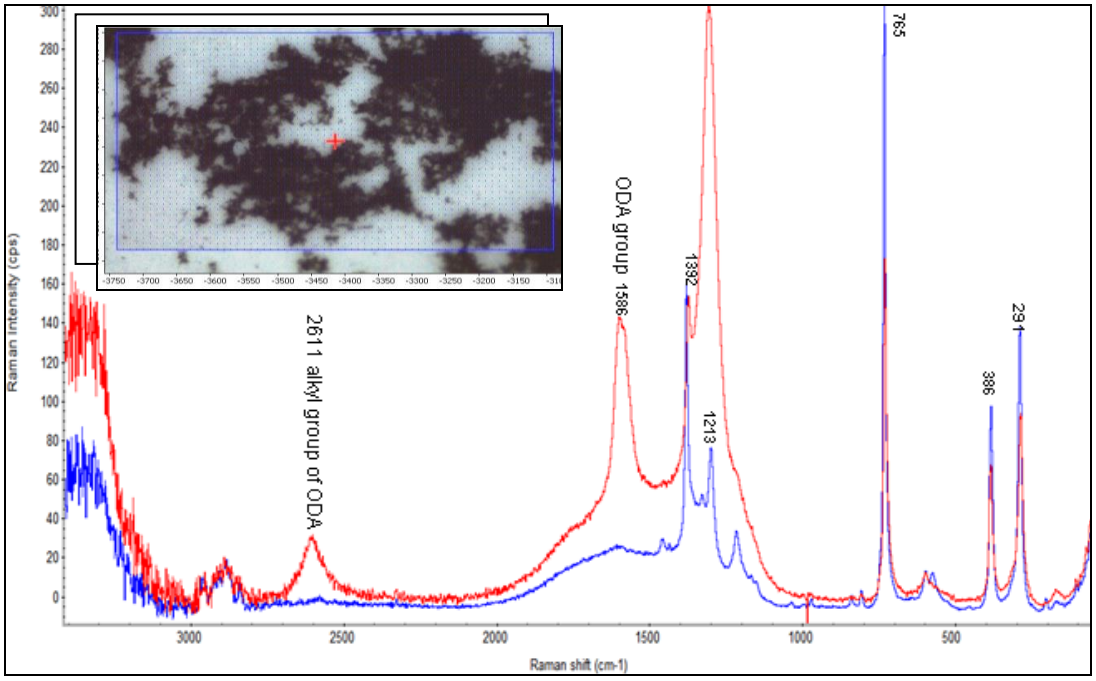

Figure 6.2 Raman Analysis Spectra of CNIM-ODA membrane.

Furthermore, Thermogravimetric analysis (TGA) was used to investigate the thermal stability of CNIM-ODA membrane material. As observed from Figure 6.3a and b, the first derivative peak at 250^{o}C and the long tail from the weight loss from 200-280^{o}C can be ascribed to the decomposition of amino groups of MWCNT-ODA. The second weight loss at around 500^{o}C and related derivate peaks are mainly attributed to the decomposition of fluorocarbon of PTFE backbone.

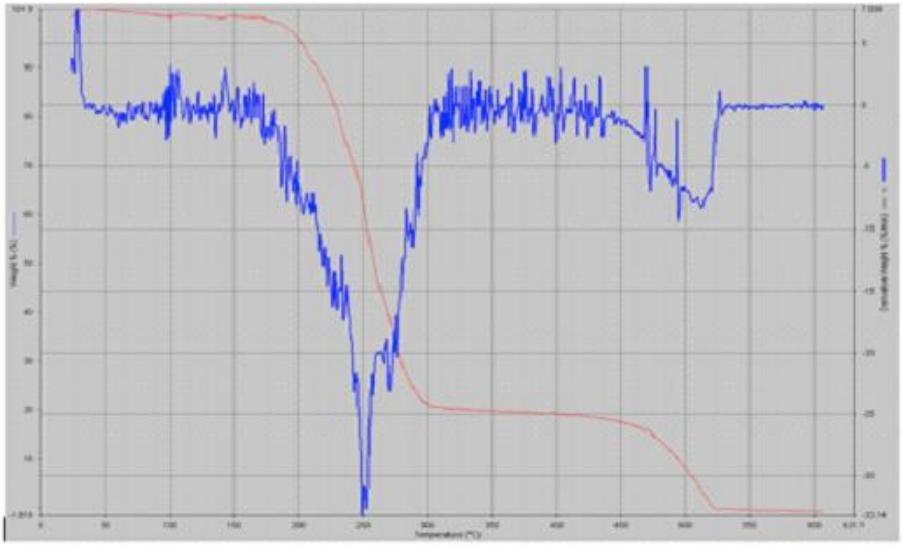

Figure 6.3 Thermal Gravimetric Analysis of CNIM-ODA membrane.

Relative hydrophobicity of membrane surfaces can be easily expressed in terms of the contact angle of deionized water. The PTFE-ODA membranes showed contact angle of 130^{o} (Figure 6.4), indicating that the hydrophobicity of PTFE membrane surface was significantly higher for CNIM-ODA as compared to unmodified PTFE membrane from Chapter 5.

Figure 6.4 Contact angle measurement of CNIM-ODA membrane.

Three sets of experiments were carried out in a traditional DCMD configuration in order

to acquire baseline performance data with the CNIM membranes (CNIM-ODA) to that of conventional unmodified PTFE membranes. These experiments evaluated the effects of feed flow rate, temperature, and concentration effect on the permeate flux.

As mentioned in previous Chapter 5, the feed operating temperature is an indispensable parameter in DCMD process as the driving force increases exponentially with elevated temperature. Temperature influence on vapor flux of the CNIM-ODA and unmodified PTFE membrane at feed flow rate 212 ml min^{-1} and distillate flow rate of 164 ml min^{-1} is depicted in Figure 6.5. As observed, the permeate fluxes exhibited an exponential dependence on feed temperature as could be expected. This could be due to the fact that temperature difference creates higher vapor pressure difference and thus the water vapor flux rises. As could be observed, maximum flux reached up to 114 kg/m^2h for CNIM-ODA. Overall, the CNIM- ODA membrane showed consistently higher flux at all temperatures among all three membrane types. This behavior of the ODA membrane could be most likely to the fact that in case of CNIM-ODA, there is a coating of additional layer of the CNT-ODA over the PTFE membrane. Due to this fact, the membrane thickness is increased which contributes to significant effects over thermodynamic effects. It is well established fact that permeability in membrane is reciprocal of membrane thickness. In our current study, the bilayer membrane was substantially thicker than the unmodified membrane and therefore the effect of the thickness at elevated temperatures overshadows the effect of the temperature on water flux. Furthermore, the PTFE membranes have rougher surfaces, especially the surface of the support layer due to the encapsulation of our polymer within the membranes, which

might further contribute to mixing at the membrane interfaces and therefore to better performance.

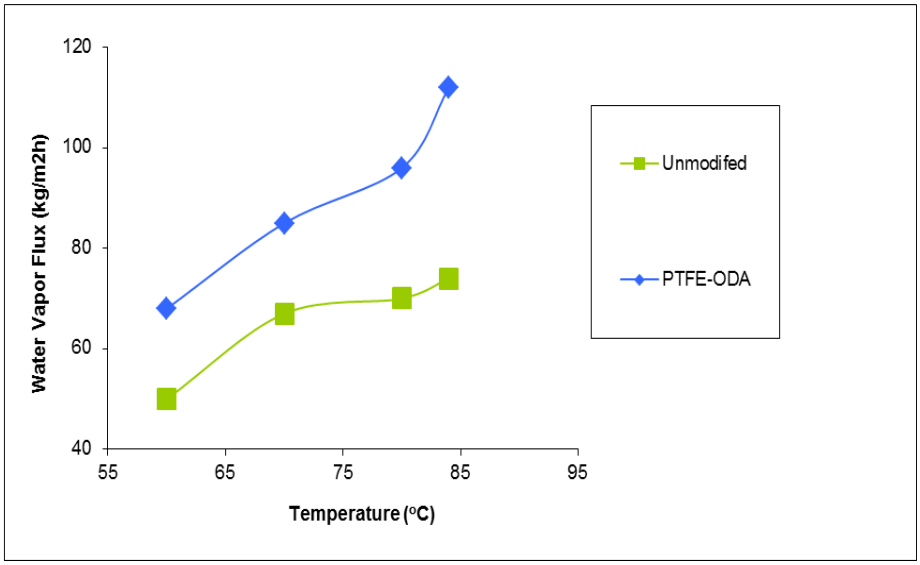

Figure 6.5 Effect of feed temperature on water vapor flux at feed flow rate 212 ml min^{-1} and distillate flow rate of 164 ml min^{-1}.

Besides feed operating temperature, another essential aspect in DCMD is the feed flow rate conditions. Figure 6.6 illustrates the performance of the modified CNIM-ODA and unmodified PTFE membrane investigated as a function of feed flow rate. During the experiments, the feed side flow rate is varied from 36 ml min^{-1} to 270 ml min^{-1} and permeate side flow rate kept constant at 164 ml min^{-1}. Salt rejection was greater than 99.9% throughout all the experiments. Results indicate that permeate flux increases with increasing feed flow rate with a maximum value reaching till 100 kg/m^2h at a feed flow rate of 270 ml min^{-1}. This was expected due to enhanced mixing in the flow channel and a decrease in the thickness of the temperature boundary layer. Typically, higher velocity

means high turbulence which will result in less temperature polarization and increased driving force across the membrane.

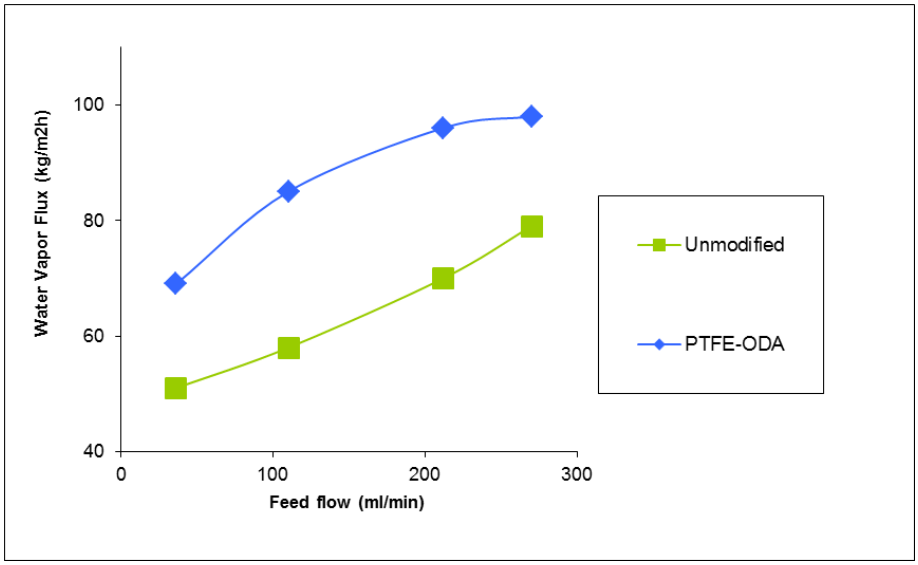

Figure 6.6 Effect of feed flow rate on water vapor flux at permeate side flow rate kept constant at 164 ml min^{-1}.

In the last set of traditional DCMD experiments, the effect of varying feed concentration on permeate flux was investigated at a feed temperature of 80^{o} C, feed flow rate of 212 ml min^{-1} and permeate flow rate of 164 ml min^{-1}. This set of data has been illustrated in Figure 6.8. Results of experiments with NaCl feed concentration ranging from 5000-34000 ppm show an average flux decline for the unmodified PTFE membrane over the investigated range. As the salt concentration increased, the vapor pressure of water decreased and these phenomena resulted in a lesser driving force for evaporation. Also, at higher feed concentration, a more significant boundary layer develops next to the membrane interface which reduces driving force of mass transfer. Consequently, this leads to the decrease in permeate flux in case of unmodified membrane. On the other

hand, the interesting aspect in regard to the observation was that, in CNIM-ODA membrane, the flux reduction was only minimal rather constant.

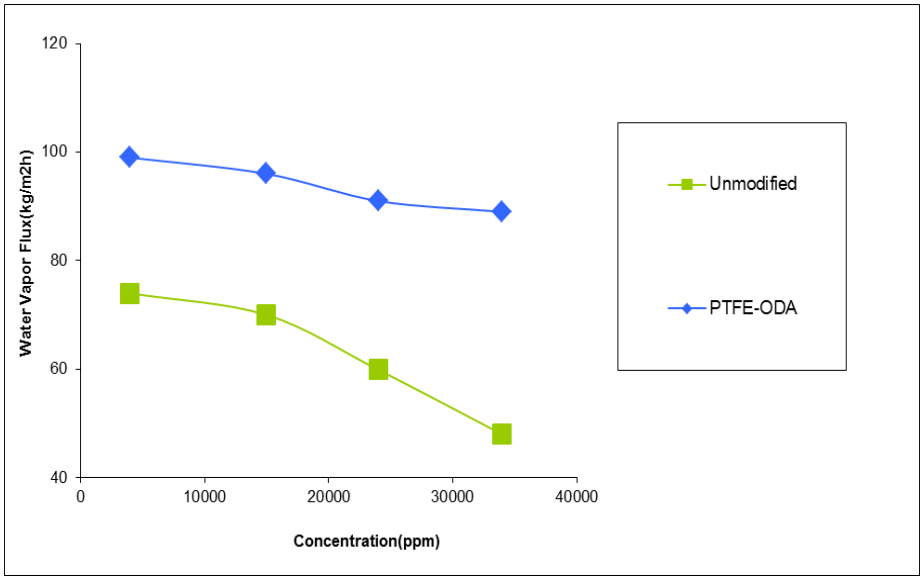

Figure 6.7 Effect of feed concentration on water vapor flux at feed temperature of 80^{o} C, feed flow rate of 212 ml min^{-1} and permeate flow rate of 164 ml min^{-1}.

6.4 Proposed Mechanism

A significantly superior flux was observed for bilayer CNIM membrane as compared to the CNIM-ODA and unmodified PTFE membrane and the mechanism is depicted in Figure 6.8. In case of the CNIM ODA membrane, the dispersion was well fabricated over the membrane surface as compared to the carboxylated fucntionalized CNIM as mentioned in Chapter 5. Hence, a uniform CNT dispersion in a well fabricated membrane would provide an enhanced route to vapor trnasport as compared to aggregation of CNTs. Further, dramatic enhancements in bilyer membrane could be attributed mainly to the fact that the octadecyl amine functionalized CNTs (CNT-ODA) are highly hydrophobic and

they increased surface hydrophobicity, enhanced the generation of vapor sites which led to higher sorption for the water vapors, consequently enhancing permeate flux. Octadecyl amine group on the MWCNT molecules consisted of carbonyl, amide as well as long alkyl octadecyl group $CH_2(CH_2)_{16}CH_3$ chains. The carbonyl and amide group initiated polar-polar interactions with the water vapor molecule thereby enhancing moisture adsorption. Overall, the C=ONH group enhanced adsorption and the $CH_2(CH_2)_{16}CH_3$ group lead to efficient desorption. The higher hydrophobicity induced by the PTFE polymer, clearly prevented water from wicking in the membrane thus potentially reducing the temperature polarization on the membrane.

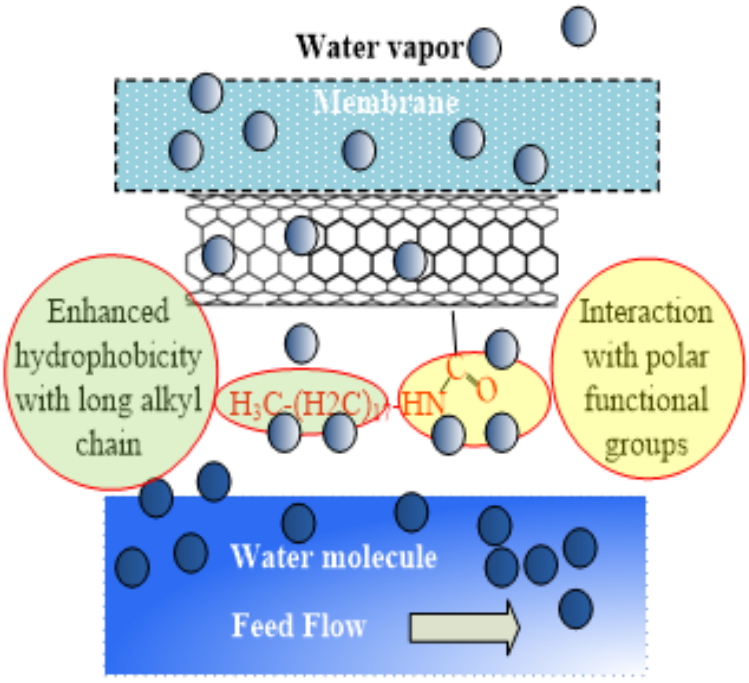

Figure 6.8 Proposed mechanism.

6.5 Conclusion

The permeate flux achieved up to a maximum of 114 kg/m^{2}hr and salt reduction higher than 99.9%. Mass transfer coefficients for CNIM-ODA membrane was significantly higher than unmodified PTFE membrane. Furthermore, the CNIM membrane also showed stability over longer period of time without any fouling and wetting issues.

REFERENCES

1. Mitra, S., Sample preparation techniques in analytical chemistry. John Wiley & Sons, Inc.; Hoboken, New Jersey, 2003.

2. Patnaik, P, Handbook of environmental analysis – chemical pollutants in air, water, soil and solid wastes. CRC Press. Boca Raton, Florida, 1997.

3. Davarani, S. H.; Pourahadi, A.; Electromembrane extraction of zwitterionic compounds as acid or base: comparison of extraction behavior at acidic and basic pHs. Anal. Chim. Acta. 2, 2012, 722.

4. Palmarsdottir, S; Mathiasson,L.; Jonsson, J. A.; Edholm, L. E., Determination of a basic drug, bambuterol, in human plasma by capillary electrophoresis using double stacking for large volume injection and supported liquid membranes for sample pretreatment. J. Chromatogr., B. 688, 1997, 127.

5. Ndungu, K., Djane, N. K.; Mathiasson, L., Determination of trace metal ions by ion-pair chromatography after enrichment using supported liquid membrane. J. Chromatogr., A. 826, 1998, 103.

6. Berhanu, T.; Liu, J. F.; Romeroa, R.; Megersa, N.; Jonsson, J. A.; Determination of trace levels of dinitrophenolic compounds in environmental water samples using hollow fiber supported liquid membrane extraction and high performance liquid chromatography. J. Chromatogr., A. 1103, 2006, 1.

7. Halvorsen, T.G.; Pedersen-Bjergaard, S.; Reubsaet, J. L. E.; Rasmussen, K. E., Liquid phase micro extraction combined with flow injection tandem mass spectrometry rapid screening of amphetamines from biological matrices. J. Sep. Sci. 24 , 2001, 615.

8. Andersen, S.; Halvorsen, T. G.; Pedersen-Bjergaard, S.; Rasmussen, K. E.; Tanum, L.; Refsum, H., Stereospecific determination of citalopram and desmethylcitalopram by capillary electrophoresis and liquid-phase microextraction. , J. Pharm. Biomed. Anal. 33 , 2003, 263.

9. Chimuka, L.; Cukrowska, E.; Jönsson, J.A., Why liquid membrane extraction is an attractive alternative in sample preparation. Pure Appl. Chem. 76, 2004, 707.

10. Hylton, K.; S. Mitra, Automated online membrane extraction. J. Chromatogr., A. 1152, 2007, 199.

11. Kathios, D.J.; Jarvinen, G. D.; Yarbro, S.L.; B. F. Smith, B. F., A preliminary evaluation of microporous hollow fiber membrane modules for the liquid-liquid extraction of actinides. J. Membr. Sci. 97, 1994, 251.

12. Bhadra, M.; Mitra, S., Nanostructured membranes in analytical chemistry. Trends in Anal. Chem. 45, 2013, 248.

13. Almeda, S.; Arce, L.; Valcarcel, M., Combined use of supported liquid membrane and solid-phase extraction to enhance selectivity and sensitivity in capillary electrophoresis for the determination of ochratoxin A in wine. Electrophoresis. 29, 2008, 1573.

14. Papaefstathiou, I. M. D.; Castro, L., Hyphenated pervaporation—solid-phase preconcentration—gas chromatography for the determination of volatile organic compounds in solid samples. J. Chromatogr., A. 779, 1997, 352.

15. Gethard, K.; Sae-Khow, O.; Mitra, S., Carbon nanotube enhanced membrane distillation for simultaneous generation of pure water and concentrating pharmaceutical waste. Sep. Purif. Technol. 90, 2012, 239.

16. Jonsson, J.A.; Mathiasson, L., Liquid membrane extraction in analytical sample preparation: I. Principles. Trends Anal. Chem. 18, 1999, 325.

17. Luthje, K.; Hyotylainen, T.; Riekkola, M. L., Determination of pesticides in red wines with on-line coupled microporous membrane liquid–liquid extraction-gas chromatography. Anal. Bioanal. Chem. 378, 2004, 1991.

18. Jonsson, J. A.; Mathiasson, L., Membrane extraction in analytical chemistry. J. Chromatogr., A. 902, 2000, 205.

19. Wang, X.; Mitra, S., Development of a total analytical system by interfacing membrane extraction, pervaporation and high-performance liquid chromatography. J. Chromatogr., A. 1068 , 2005, 237.

20. Curcio, E., Drioli, E., Membrane distillation and related operations- a review. Sep. and Pur. Rev. 34, 2005, 35.

21. Alklaibi, A.; Lior, N., Membrane-distillaiton desalination: status and potential. Desal. 171, 2004, 111.

22. Zimmerman, C. M.; Singh, A.; Koros. W. J., Tailoring mixed matrix composite membranes for gas separations. J. Membr. Sci. 2, 1997, 145.

23. Sholl, D. S.; Johnson, J. K., Fast mass transport through sub-2-nanometer carbon nanotubes. Science. 312, 2006, 1003.

24. Hinds, B. J.; Chopra, N.; Rantell, T.; Andrews, R.; Gavalas, V.; Bachas, L. G., Aligned multiwalled carbon nanotube membranes. Science. 303, 2004, 62.

25. Gethard, K.; Sae-Khow, O.; Mitra, S., Water desalination using carbon-nanotube-enhanced membrane distillation. Appl. Mater. Interfaces. 3, 2011, 110.

26. Hylton, K.; Chen,Y.; Mitra, S., Carbon nanotube mediated microscale membrane extraction. J. Chromatogr., A. 1211, 2008, 43.

27. Peng, F.; Hu, C., Novel ploy (vinyl alcohol)/carbon nanotube hybrid membranes for pervaporation separation of benzene/cyclohexane mixtures. J. Membr. Sci. 297, 2007, 236.

28. Lee, P. K.; Arnot, T, C., A review of reverse osmosis membrane materials for desalination—development to date and future potential. J. Membr. Sci. 370, 2011, 1.

29. Bhadra, M.; Mitra, S.; Carbon nanotube immobilized polar membranes for enhanced extraction of polar analytes. Analyst. 137, 2012, 4464.

30. Hylton, K.; Mitra, S., Automated, on-line membrane extraction. J. Chromatogr., A. 2007, 1152, 199.

31. Mo, K. B., Membrane-based solvent extraction for selective removal and recovery of metals. Membrane Science. 198, 21, 5.

32. Basheer, C.; Lee, H. K.; Development and application of porous membrane-protected carbonnanotube micro-solid-phase extraction combined with gas chromatography/mass spectrometry. J. Chromatogr., A. 1047, 2004, 189.

33. Wang, X.; Saridara, C.; Mitra, S., Microfluidic supported liquid membrane extraction.Anal. Chim. Acta. 543, 2005, 92.

34. Kou, D.; Wang, X.; Mitra. S., Supported liquid membrane microextraction with high-performance liquid chromatography–UV detection for monitoring trace haloacetic acids in water.J. Chromatogr., A. 2004, 1055, 63.

35. Wang, X.; Kou, D.; Mitra, S., Continuous, on-line monitoring of haloacetic acids via membrane extraction. J. Chromatogr., A. 1089, 2005, 39.

36. Rasmussen, K. E.; Pedersen-Bjergaard, S., Developments in hollow fibre-based, liquid-phase microextraction. Trends Anal. Chem. 23, 2004, 1.

37. Hylton, K.; Mitra, S., Barrier film protected, and mixed solvent optimized micro-scale membrane extraction of methyl carbamate pesticides. J. of Chromatogr., A. 1154, 2007, 60.

38. Sae-Khow, O.; Mitra, S., Fabrication and characterization of carbon nanotubes immobilized in porous polymeric membranes. J. Mater. Chem. 19, 2009, 3713.

39. Tan, F.; Deng, F.; Liu, X.; Zhao, H.; Li, X.; Quan, X.; Chen, J.; Evaluation of a novel microextraction technique for aqueous samples: Porous membrane envelope filled with multiwalled carbon nanotubes coated with molecularly imprinted polymer. J. Sep. Sci. 34, 2011, 707.

40. Wang, Y.; Iqbal, Z.; Mitra, S., Microwave-induced rapid chemical functionalization of single-walled carbon nanotubes .Carbon. 43, 2005, 1015.

41. Luthhje, K.; Hyötyläinen, T.; Riekkola, M. L., On-line coupling of microporous membrane liquid–liquid extraction and gas chromatography in the analysis of organic pollutants in water. Anal. Bioanal. Chem. 378, 2004, 1991.

42. Juang, R.S.; Kao, H.C.; Wu, W.H., Analysis of liquid membrane extraction of binary Zn (II) and Cd (II) from chloride media with Aliquat 336 based on thermodynamic equilibrium models. J. Membr. Sci. 228, 2004, 169.

43. Hou, L.; Shen, G.; Lee, H. K., Automated hollow fiber-protected dynamic liquid-phase microextraction of pesticides for gas chromatography–mass spectrometric analysis. J. Chromatogr., A. 985, 2003, 107.

44. Hou, L.; Lee, H. K., Application of static and dynamic LPME in the determination of polycyclic aromatic hydrocarbons. J. Chromatogr., A. 976, 2002, 377.

45. Delgado-Torres, A. M.; Rodriguez, L. G., Status of solar thermal-driven reverse osmosis desalination, Desal. 216, 2007, 242.

46. Khawaji, A.D.; Kutubkhana, I. K.; Wie, J. M., Advances in seawater desalination technologies, Desal. 221, 2008, 47.

47. Peñate, B.; Rodríguez, L. G., Current trends and future prospects in the design of seawater reverse osmosis desalination technology, Desal. 284, 2012, 1.

48. Misdan, N.; Lau, W. J.; Ismail, A.F., Seawater Reverse Osmosis (SWRO) desalination by thin-film composite membrane-Current development, challenges and future prospects, Desal. 287, 2012, 228.

49. Li, M., Optimal plant operations of brackish water reverse osmosis (BWRO) desalination, Desal. 293, 2012, 61.

50. Sablani, S.S. ; Goosen, M. F. A. ; Al-Belushi, R. ; Wilf, M., Concentration polarization in ultrafiltration and reverse osmosis: a critical review, Desal. 141, 2001, 269.

51. Peng, P.; Fane, A.G.; Li, X., Desalination by membrane distillation adopting a hydrophilic membrane, Desal. 173, 2005, 45.

52. Babu, B. R.; Rastogi, N.K.; Raghavarao, K. S., Concentration and temperature polarization effects during osmotic membrane distillation, J Membr. Sci. 322, 2008, 146.

53. College of Engineering, University of Texas at El Paso**,** Desalination water purification research and development program, Report No. 81, 2004.

54. Khemakhem, S.; Amar, R. B., Modification of tunisian clay membrane surface by silane grafting: application for desalination with air gap membrane distillation process, Colloids. Surfaces. A: Physicochemical. Eng. Aspects. 387, 2011, 79.

55. Fang, H.; Gao, J. F.; Wang, H. T.; Chen, C. S., Hydrophobic porous alumina hollow fiber for water desalination via membrane distillation process, J. Membr. Sci. 403, 2012, 41.

56. Ong, Y. T.; Ahmad, A.L.; Zein, S. H.S.; Sudesh, K.; Tan, S. H., Poly(3-hydroxybutyrate)-functionalised multi-walled carbon nanotubes/chitosan green nanocomposite membranes and their application in pervaporation, Sep. Purif. Technol. 76, 2011, 419.

57. Peng, F.; Hu, C.; Jiang, Z., Novel poly (vinyl alcohol)/carbon nanotube hybrid membranes for pervaporation separation of benzene/cyclohexane mixtures, J. Membr. Sci. 297, 2007, 236.

58. Jia, Y. X.; Li, H. L.; Wang, M.; Wu, L. Y.; Hu, Y. D., Carbon nanotube: possible candidate for forward osmosis, Sep. Purif. Technol. 75, 2010, 55.

59. Roy, S.; Ntim, S. A.; S. Mitra, S.; K.K. Sirkar, K. K., Facile fabrication of superior nanofiltration membranes from interfacially polymerized CNT-polymer composites, J. Membr. Sci. 375, 2011, 81.

60. Vatanpour, V.; Madaeni, S. S.; Moradian, R.; Zinadini, S.; Astinchap, B., Fabrication and characterization of novel antifouling nanofiltration membrane prepared from oxidized multiwalled carbon nanotube/polyethersulfone nanocomposites, J. Membr. Sci. 375 , 2011, 284.

61. Manikandan, D.; Mangalaraja, R, V.; Siddheswaran, R.; Avila, R. E.; Ananthakumar, S., Fabrication of nanostructured clay–carbon nanotube hybrid nanofiller by chemical vapour deposition, Appl. Surf. Sci. 258, 2012, 4460.

62. Bhadra, M.; Roy, S.; Mitra, S., Enhanced desalination using carboxylated carbon nanotube membrane, Sep. Purif. Technol. 120, 2013, 373.

63. Mochalin, V. N.; Shenderova, O.; Ho, D.; Gogotsi, Y., The properties and applications of nanodiamonds, Nature Nanotechnol. 7, 2012, 11.

64. Dubois, M.; Guerin, K., Solid state NMR study of nanodiamond surface chemistry, Solid State Nucl Magn Reson. 40, 2011, 144.

65. He, D.; Shao,U. L.; Gong, W.; Xiea, E.; Xu, K.; Chen. G., Electron transport and electron field emission of nanodiamond synthesized by explosive detonation, Diamond. Relat. Mater. 9 , 2000, 1600.

66. Dolmatov, V. Y., Ultradisperse diamonds produced by detonation synthesis: properties and applications, Russ. Chem. Rev. 70, 2001, 607.

67. Wang, D.H.; Tan, L.S.; Huang, H.J.; Dai, L.M.; Osawa, E., In-situnanocomposite synthesis: Arylcarbonylation and grafting of primary diamond nanoparticles with a poly (ether–ketone) in polyphosphoric acid, Macromolecules. 42, 2009, 114.

68. Cheng, J. L.; He, J.P.; Li, X. C.; Yang, Y.L., Facile approach to functionalize nanodiamond particles with V-shaped polymer brushes, Chem. Mater. 20, 2008, 4224.

69. Mochalin , V. N.; Neitzel ,I.; Etzold , B.J.; Peterson ,A.; Palmese , G.; Gogotsi , Y., Covalent incorporation of nanodiamond in epoxy network, ACS Nano. 5, 2011, 7494.

70. Shimkunas, R. A., Nanodiamond–insulin complexes as pH-dependent protein delivery vehicles, Biomaterials. 30, 2009, 5720.

71. Purtov, K.V.; Petunin, A. I.; Burov, A. E.; A. P. Puzyr, A. P.; Nanodiamonds as carriers for address delivery of biologically active substances, Nanoscale Res. Lett. 5**,** 2010, 631.

72. Alhaddad, A., Nanodiamond as a vector for siRNA delivery to ewingsarcoma cells, Small. 2011, 7, 3087.

73. Wei, L.; W. Zhang, W.; Immobilization of enzyme on detonation nanodiamond for highly efficient proteolysis, Talanta. 80, 2010, 1298.

74. Zhang, X. Q.; M. Chen, M., Polymer-functionalized nanodiamond platforms as vehicles for gene delivery, ACS Nano. 2009, 3, 2609.

75. Zhang, Q. X.; Lam, R.; Xu, X.; Chow, E. K.; Kim, H. J.; Ho, D.; Multimodal nanodiamond drug delivery carriers for selective targeting, imaging, and enhanced chemotherapeutic efficacy, Adv. Mater. 23, 2011, 4770.

76. Yeap, W. S.; Tan, Y. Y.; Using detonation nanodiamond for the specific capture of glycoproteins, Anal. Chem. 80 ,2008, 4659.

77. Bhadra, M.; Roy, S.; Mitra, S., Nanodiamond immobilized membranes for enhanced desalination via membrane distillation, Desal. DOI. 10.1016/j.desal.2014.02.036.

78. Desai, C.; Mitra, S., Microwave induced carboxylation of nanodiamonds, Diam. Relat. Mater. 34, 2013, 65.

79. Hsu, S. T.; Cheng, K. T.; Chiou, J. S. Seawater desalination by direct contact membrane distillation. Desal. 143, 2002, 279.

80. Cath, T. Y.; Dean Adams, V.; Childress, A. E. Experimental study of desalination using direct contact membrane distillation: a new approach to flux enhancement. J Membr. Sci., 228, 2004, 5.

81. Qtaishata, M.; Matsuuraa, T.; Kruczeka, B.; Khayet, M. Heat and mass transfer analysis in direct contact membrane distillation. Desal. 219, 2008, 272.

82. Phattaranawik, J.; Jiraratananon, R. Direct contact membrane distillation: effect of Mass transfer on heat transfer. J. Membr. Sci. 188, 2001, 137.

83. Singh, D.; Sirkar, K. K., Desalination of brine and produced water by direct contact membrane distillation at high temperatures and pressures. J. Membr. Sci. 389, 2012, 380.

84. Mihaly, J.; Sterkel, S.; Ortner, H. M.; Kocsis, L.; Hajba, E.; Furdyga, E; Minka, FTIR and FT-Raman spectroscopic study on polymer based high pressure digestion vessels . J. Croatica. Chemica. Acta. 79, 2006, 497-501.

85. Khayet, M.; Matsuraa, T., Membrane distillation principle and applications; Elsevier : 2011, Chapter 10, 249.

86. Shirazi, M; Kargari. A.; Bastani , D.; Fatehi, L. Production of drinking water from seawater using membrane distillation (MD) alternative: direct contact MD and sweeping gas MD approaches. Desalination and water treatment. 1, 2013, 10.

87. Hwang, H.; He, K.; Gray, S.; Zhang, J.; Moon, S., Direct contact membrane distillation (DCMD): Experimental study on the commercial PTFE membrane and modeling. Jr. Membr. Sci. 371, 2011, 90.